Merging of the α and β relaxations in polybutadiene: A neutron spin echo and dielectric study

A. Arbe and D. Richter
Institut für Festkörperforschung, Forschungszentrum Jülich, 52425 Jülich, Germany

J. Colmenero
Departamento de Física de Materiales, Universidad del País Vasco, Apartado 1072, 20080 San Sebastián, Spain

B. Farago
Institut Laue-Langevin, 156X, 38042 Grenoble Cedex, France
(Received 26 February 1996)

The local dynamics of 1,4 polybutadiene below and above the merging of the α and β relaxations have been investigated by combining neutron spin echo (NSE) and dielectric spectroscopy. The study of the dynamic structure factor measured by NSE over a wide momentum transfer range allows us to characterize the α relaxation as an interchain process while the β relaxation originates from mainly intrachain motions. At temperatures below the merging, the dynamic structure factor can be described by a superposition of elemental processes for the β relaxation as obtained from dielectric spectroscopy. The elemental motions behind this process can be related to rotational jumps of the chain building blocks around their center of mass. Furthermore, we have been able to consistently describe the dynamic structure factor above the merging of the α and β relaxations by assuming that both processes are statistically independent. In the framework of this scenario a procedure for analyzing the dielectric response in the α-β merging region has been developed. Its application to the dielectric data allows us to describe the dielectric response in this region on the basis of the low temperature behavior of the α and β processes and without considering any particular change in the relaxation mechanism of these processes. The temperature dependence found for the relaxation time of the α process follows now the viscosity, a masked feature in the experimental data due to the merging process. In this way, we have been able to consistently describe the relaxation of both, the polarization and the density fluctuations, by using the same scenario, i.e., independent α and β processes, and considering the same functional forms and temperature dependences of the characteristic times of the two processes. [S1063-651X(96)07209-1]

PACS number(s): 61.20.−p, 64.70.Pf, 61.12.Ex, 61.41.+e

I. INTRODUCTION

It is well established that (at least) two relaxational processes take place in all glass-forming polymers [1,2]: the primary or structural α relaxation and the secondary or β relaxation, also known as the Johari-Goldstein process [3]. Both of these relaxations coalesce in what we will call the α-β process in a temperature range 10%–20% above the glass transition temperature T_g, which we will refer to as the merging temperature T_M. The α relaxation is commonly believed to be related to segmental relaxations of the main chain. The temperature dependence of its relaxation time shows a dramatic increase around T_g, leading to the glassy state at lower temperatures. The β relaxation is active above as well as below T_g, and occurs independently of the existence of side groups in the polymer. This relaxation has traditionally been attributed to local relaxation of flexible parts, e.g., side groups, and, in main chain polymers, to twisting or crankshaft motion in the main chain [1]. On the other hand, the origin of the α relaxation should be of an intermolecular nature in the context of some models of the glass transition [4]. The molecular nature of the secondary relaxation and its relationship with the primary relaxation are still unknown.

The dynamics of glass-forming systems have mainly been investigated by means of relaxation techniques like dielectric spectroscopy or dynamical mechanical measurements. In order to access the relaxational processes on a molecular level, it is necessary to get spatial information of the relaxations. Through the momentum transfer (Q) dependence of the dynamic structure factor $S(Q,t)$ this information can be provided by quasielastic neutron scattering (QENS) techniques. Because it measures directly in the time domain, neutron spin echo (NSE) is a particularly well suited QENS technique for this task. Up to now most of the NSE experiments on glass-forming liquids have been performed in a temperature range above the merging of the α and β relaxations in a relatively narrow Q range near the first peak of the static structure factor $S(Q)$ [5,6], where the spectra are mainly dominated by intermolecular correlations. These experiments have established the validity of the time-temperature superposition principle and the existence of one universal temperature scale, which is valid for both viscosity relaxation and density fluctuations. However, later NSE experiments on 1,4 polybutadiene (PB) performed near the first minimum of $S(Q)$ [7] revealed two interesting results: on the one hand, the spectral shape was different from the observed one at the first peak [6], and, on the other hand, a decoupling of the microscopic time scale from the time scale set by the viscosity relaxation was observed. Dielectric measurements brought evidence that below the decoupling temperature, which coincides with T_M for this polymer, the NSE relaxations appear to correspond to the β process [8]. In a recent work [9], we have investigated the dynamic structure factor in the β-relaxation regime of 1,4 PB, including new measurements performed at Q values close to the second maximum of $S(Q)$ the intrachain peak [10]. We found that the

dynamics in this Q range is dominated by the β relaxation, leading to an assignment of an intramolecular origin to this relaxation. In that work we described the NSE data-below T_M in terms of a localized motion occurring on a length scale of about 1.5 Å with the barrier distribution from dielectric spectroscopy. Now, knowing that the β-relaxation contributes to the decay of the density fluctuations measured by NSE, the question arises, what can be learned from the NSE data in the merging regime and above on the relation between these two relaxation processes.

The investigation of the dynamics in the merging region of the α and β relaxations is a subject of great interest, because it may shed some light on the nature of both processes. Concerning dielectric investigations on polymeric systems, the understanding of the dynamics in this region is still poor, partly due to the difficulty to access experimentally its frequency range ($\approx 10^6$–10^8 Hz), lying in the upper limit of standard relaxation techniques, but mainly as a consequence of the missing spatial information. A phenomenological description of possible scenarios for the α-β splitting has been made [11], but this study has been based on the traditional analysis of dielectric data, i.e., by assuming that the spectra can be described by the addition of the contributions corresponding to the α and β relaxations. This analysis implies that there are two kinds of dipoles, each of them relaxing through one of the two processes. As far as we know, any other kind of treatment of dielectric data has not been yet quantitatively performed. Moreover, in the particular case of 1,4 PB the temperature dependence of the dielectric time scale deduced from the maxima of the dielectric loss, usually assigned to the α relaxation, does not follow the temperature behavior of the time scale associated with the viscosity, as would be expected. This is another open question which could be addressed in the framework of the description of the merging process.

In this work we present a study of the dynamics of the glass-forming polymer 1,4 PB at temperatures below and above the merging of the α and β relaxations. For this purpose we have combined NSE and broadband dielectric techniques. While the last one facilitates precise information about the temperature dependence of the characteristic times and the spectral shape of the relaxations, NSE provides space-time information about the processes involved in the mesoscopic dynamics of the system, but compared to dielectric spectroscopy its dynamic range is rather limited. Therefore, a combination of both methods is necessary to achieve further progress in the understanding of the mechanisms beyond the dynamics of the α, β, and α-β relaxations in glass-forming systems. Analyzing the merging process we show that α and β relaxations appear to be statistically independent. This result is supported by a recent study of these relaxations in PBs of varying microstructure [12]. Such an independence of α and β relaxations was already suggested by Williams [13] for dielectric relaxation, but has never been quantitatively checked. In Sec. II we present some theoretical results about coherent structure factors for different types of localized motions and for the merging of two processes. Thereafter, the NSE and the dielectric spectroscopy studies are reported.

II. NEUTRON SPIN ECHO STUDY: THEORETICAL CONSIDERATIONS

In general NSE experiments explore the coherent intermediate dynamic structure factor [14] relating to the pair correlation function of the moving atoms. In contrast, QENS experiments on localized motions are generally performed by incoherent scattering yielding the self-correlation function. This is due to mainly two reasons: (i) Hydrogen (large incoherent cross section) is the most investigated atom, and (ii) the interpretation of incoherent scattering functions, revealing the single particle motion, is much more simple than the coherent case, which addresses the relative motion of different particles. Therefore, the coherent scattering function has been much less investigated than its incoherent counterpart. In order to lay the grounds for an analysis of the NSE data in terms of model coherent scattering functions, in the following we consider QENS from coherently scattering atom configurations performing simple jump processes. These considerations are the basis for an interpretation of scattering from the localized β relaxation (Sec. II A). In order to deal also with the merging of α and β relaxation in Sec. II B we approximate the coherent structure factor for atom configurations undergoing two different statistically independent processes.

A. Coherent scattering function for localized motions

In the following we will consider a two-level system with energetically equal levels. One scatterer undergoes transitions between two positions, labeled as 1 and 2 (position vectors $\vec{r}_1$ and $\vec{r}_2$), with a transition rate $1/\tau$. Let $P_{ij}(t)$ (with $i,j=1,2$) be the conditional probability of finding the scatterer at position j at time t if at $t=0$ it was at position i. It is easy to find that

$$P_{11}(t)=P_{22}(t)=\tfrac{1}{2}(1+e^{-2t/\tau}), \tag{1a}$$

$$P_{12}(t)=P_{21}(t)=\tfrac{1}{2}(1-e^{-2t/\tau}). \tag{1b}$$

The incoherent intermediate scattering function can be written as

$$S(Q,t)=\langle e^{i\vec{Q}\cdot[\vec{r}(t)-\vec{r}(0)]}\rangle=\sum_{i,j} P_i^0 P_{ij}(t)\langle e^{i\vec{Q}\cdot(\vec{r}_j-\vec{r}_i)}\rangle, \tag{2}$$

where P_i^0 is the probability of finding the scatterer at i at $t=0$. For energetically equal levels we have $P_1^0=P_2^0=1/2$. Taking an average over all the possible orientations of the vector $\vec{r}_j-\vec{r}_i$ with respect to $\vec{Q}$, i.e.,

$$\langle e^{i\vec{Q}\cdot(\vec{r}_j-\vec{r}_i)}\rangle=\frac{\sin(Q|\vec{r}_j-\vec{r}_i|)}{Q|\vec{r}_j-\vec{r}_i|}, \quad i\neq j \tag{3}$$

we can deduce from Eqs. (1) and (2) that the incoherent scattering function for such a system is given by

$$S(Q,t)=\frac{1}{2}\left[1+\frac{\sin(Qd)}{Qd}\right]+\frac{1}{2}\left[1-\frac{\sin(Qd)}{Qd}\right]e^{-2t/\tau}, \tag{4}$$

where $d=|\vec{r}_j-\vec{r}_i|$ is the jump distance.

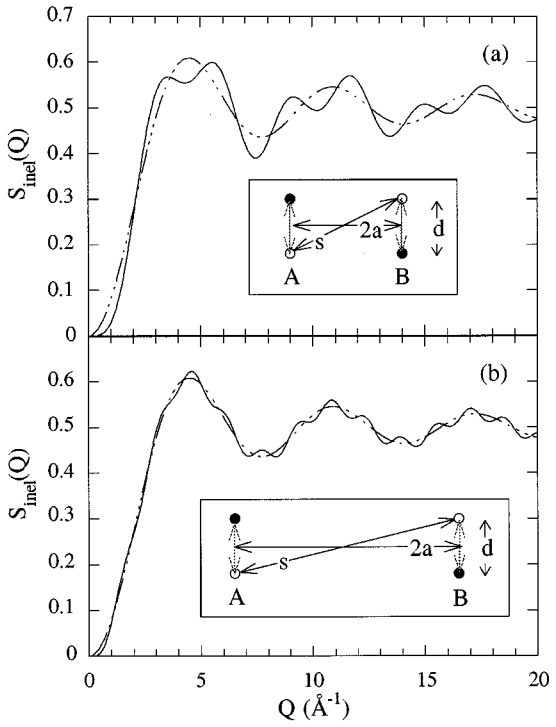

FIG. 1. Inelastic contribution to the scattering function in the incoherent (dashed-dotted line) and coherent (solid) cases for correlated hopping processes. The jump distance d is 1 Å and the distance $2a$ between correlated particles are 2 Å (a) and 4 Å (b).

Now we will build the coherent structure factor of hopping pairs. Let us consider two scatterers, labeled as A and B, which perform transitions between two positions (see as an example insets in Fig. 1). We will treat two different cases: (i) correlated and (ii) uncorrelated jumps.

The basic difference in calculating the coherent scattering function compared to its incoherent counterpart relates to the problem that other than for incoherent scattering, where the motion of one particular atom is traced, now we have to treat the scattering from changing atom configurations: we have to consider all possible initial and final states, calculate their scattering amplitudes, take the appropriate products of amplitudes and perform the necessary averages.

Our pair of atoms A and B may assume the positions $\vec{r}_{A_1}$, $\vec{r}_{A_2}$, and $\vec{r}_{B_1}$ and $\vec{r}_{B_2}$, respectively. If (i,j) and (l,k) designate the initial and final atom configurations, respectively, $(i,j,k,l=1,2)$, the scattering amplitudes for these two states are

$$A_{ij}(Q)=e^{i\vec{Q}\cdot\vec{r}_{A_i}}+e^{i\vec{Q}\cdot\vec{r}_{B_j}}, \tag{5a}$$

$$A_{lk}(Q)=e^{i\vec{Q}\cdot\vec{r}_{A_1}}+e^{i\vec{Q}\cdot\vec{r}_{B_k}}. \tag{5b}$$

The form factors $F_{lk}^{ij}(Q)$ describing the different configurations then are given by

$$F_{lk}^{ij}(Q)=[A_{ij}(Q)]^{*}A_{lk}(Q). \tag{6}$$

Now we consider the case of correlated hopping of atomic pairs. We have to distinguish two different initial and final states, respectively. If the initial and final states are identical, that is, no transition took place, then $P_{11}(t)$ or $P_{22}(t)$ describe the corresponding probabilities. For the case that a transition occurred, $P_{12}(t)$ or $P_{21}(t)$ are the probability functions. With Eqs. (1), (5), and (6) the coherent structure factor becomes

$$\begin{aligned}S(Q,t)=&\tfrac{1}{2}\{\tfrac{1}{2}P_{11}(t)[A_{11}(Q)]^{*}A_{11}(Q)+\tfrac{1}{2}P_{22}(t)\\&\times[A_{22}(Q)]^{*}A_{22}(Q)+\tfrac{1}{2}P_{12}(t)[A_{11}(Q)]^{*}A_{22}(Q)\\&+\tfrac{1}{2}P_{21}(t)[A_{22}(Q)]^{*}A_{11}(Q)\}\end{aligned} \tag{7a}$$

$$\begin{aligned}=&\tfrac{1}{4}|A_{11}(Q)+A_{22}(Q)|^2\\&+\tfrac{1}{4}|A_{11}(Q)-A_{22}(Q)|^2e^{-2t/\tau}.\end{aligned} \tag{7b}$$

Here we have already introduced the initial condition of equal probability of finding the particles in each possible position at time 0. The global factor 1/2 arises from the normalization of $S(Q,t)$ to the number of atoms.

As an example we consider the case illustrated in the inset of Fig. 1 where a pair of atoms moves in counter sense. In this case the center of mass of the moving system is fixed; the positions of the scatterers are given by: $\{A_1\}:(-a,-d/2)$; $\{B_1\}:(a,d/2)$; $\{A_2\}:(-a,d/2)$; $\{B_2\}:(a,-d/2)$. Let us call $s=\sqrt{d^2+4a^2}$ (see insets of Fig. 1). Taking an isotropic average [Eq. (3)], and taking into account that $|\vec{r}_{A_1}-\vec{r}_{B_1}|=|\vec{r}_{A_2}-\vec{r}_{B_2}|=s$; $|\vec{r}_{A_1}-\vec{r}_{A_2}|=|\vec{r}_{B_1}-\vec{r}_{B_2}|=d$; $|\vec{r}_{A_1}-\vec{r}_{B_2}|=|\vec{r}_{A_2}-\vec{r}_{B_1}=2a$, the coherent structure factor deduced from Eq. (7) reads

$$\begin{aligned}S(Q,t)=&\frac{1}{2}\left[1+\frac{\sin(Qs)}{Qs}+\frac{\sin(Qd)}{Qd}+\frac{\sin(2Qa)}{2Qa}\right]\\&+\frac{1}{2}\left[1+\frac{\sin(Qs)}{Qs}-\frac{\sin(Qd)}{Qd}-\frac{\sin(2Qa)}{2Qa}\right]e^{-2t/\tau}.\end{aligned} \tag{8}$$

A simple case where the center of mass moves is realized by: $\{A_1\}:(-a,-d/2)$; $\{B_1\}:(a,-d/2)$; $\{A_2\}:(-a,d/2)$; $\{B_2\}:(a,d/2)$, and the corresponding distances are $|\vec{r}_{A_1}-\vec{r}_{B_1}|=|\vec{r}_{A_2}-\vec{r}_{B_2}|=2a$; $|\vec{r}_{A_1}-\vec{r}_{A_2}|=|\vec{r}_{B_1}-\vec{r}_{B_2}|=d$; $|\vec{r}_{A_1}-\vec{r}_{B_2}|=|\vec{r}_{A_2}-\vec{r}_{B_1}|=s$. The spatial average of Eq. (7) results in the following expression for the coherent structure factor:

$$\begin{aligned}S(Q,t)=&\frac{1}{2}\left[1+\frac{\sin(2Qa)}{2Qa}+\frac{\sin(Qd)}{Qd}+\frac{\sin(Qs)}{Qs}\right]\\&+\frac{1}{2}\left[1+\frac{\sin(2Qa)}{2Qa}-\frac{\sin(Qd)}{Qd}-\frac{\sin(Qs)}{Qs}\right]e^{-2t/\tau}.\end{aligned} \tag{9}$$

In the case of uncorrelated motion which we now consider the two scatterers A and B jump independently from each other. Therefore, the dynamic structure factor involves the products of the transition probabilities of both particles A and B, $P_{ij}^{A}(t)$ and $P_{ij}^{B}(t)$, $i,j=1,2$, respectively,

$$S(Q,t)=\frac{1}{2}\frac{1}{4}\sum_{\substack{i,j\\k,l}} P_{ij}^{A}(t)P_{kl}^{B}(t)[A_{ik}(Q)]^{*}A_{jl}(Q), \quad (10)$$

where the factors 1/2 and 1/4 correspond to the normalization of $S(Q,t)$ to the number of particles and to the product of the initial probability conditions (assumed to be equal for both particles and both positions), respectively. Equation (10) contains 16 contributions; taking the isotropic averages, their sum can be calculated to be

$$\frac{1}{4}(1+e^{-2t/\tau})^{2}\left[1+\frac{1}{2}\frac{\sin(2Qa)}{2Qa}+\frac{1}{2}\frac{\sin(Qs)}{Qs}\right] \quad (11a)$$

$$+\frac{1}{4}(1-e^{-4t/\tau})\left[1+\frac{\sin(2Qa)}{2Qa}+\frac{\sin(Qs)}{Qs}+\frac{\sin(Qd)}{Qd}\right] \quad (11b)$$

$$+\frac{1}{4}(1-e^{-2t/\tau})^{2}\left[\frac{\sin(Qd)}{Qd}+\frac{1}{2}\frac{\sin(2Qa)}{2Qa}+\frac{1}{2}\frac{\sin(Qs)}{Qs}\right], \quad (11c)$$

where contribution (11a) comes from the terms $i=j$, $k=l$; (11b) from the terms $i=j$, $k\neq l$ and $i\neq j$, $k=l$, and (11c) from the terms $i\neq j$, $k\neq l$. The final expression for $S(Q,t)$ follows as:

$$S(Q,t)=\frac{1}{2}\left[1+\frac{\sin(2Qa)}{2Qa}+\frac{\sin(Qd)}{Qd}+\frac{\sin(Qs)}{Qs}\right]+\frac{1}{2}\left[1-\frac{\sin(Qd)}{Qd}\right]e^{-2t/\tau}. \quad (12)$$

From inspection and comparison of the structure factors we observe: For $t=0$ and correlated motion we find the Fourier transform of a dumbbell of length s or $2a$, respectively,

$$S(Q,0)=1+\frac{\sin\{Qs,2Qa\}}{\{Qs,2Qa\}} \quad (13)$$

and in the uncorrelated case we find a mixture of both corresponding to an equal population of distances s and $2a$

$$S(Q,0)=\frac{1}{2}\left[1+\frac{\sin(Qs)}{Qs}\right]+\frac{1}{2}\left[1+\frac{\sin(2Qa)}{2Qa}\right]. \quad (14)$$

For $t=\infty$, which for incoherent scattering corresponds to the elastic incoherent structure factor, the result is the same in the three cases

$$S(Q,\infty)=\frac{1}{2}\left[1+\frac{\sin(Qs)}{Qs}+\frac{\sin(2Qa)}{2Qa}+\frac{\sin(Qd)}{Qd}\right], \quad (15)$$

i.e., the particles are equally distributed among the four sites.

Concerning the inelastic part, in the uncorrelated case we recuperate the incoherent result, whereas for correlated motions the incoherent inelastic contribution is complemented by

$$\pm\frac{1}{2}\left[\frac{\sin(Qs)}{Qs}-\frac{\sin(2Qa)}{2Qa}\right]. \quad (16)$$

It can be seen easily that if the distance between correlated jumping atoms is large compared to the jump distance d, these modifications of the inelastic form factor [Eq. (16)] stay small. As an example, Fig. 1 compares the inelastic contributions to $S(Q,t)$ for the incoherent case with that for correlated motion [Eq. (8)] for a jump distance $d=1$ Å assuming $a=1$ Å [Fig. 1(a)], and $a=2$ Å [Fig. 1(b)]. It is evident that the deviations between coherent and incoherent form factors reduce strongly with increasing difference between the distance of the hopping pairs compared to the jump length.

Let us now consider transitions of a rigid object between two levels, where again the transition probabilities are described by Eq. (1). The object may contain N atoms with the scattering length b_i at positions $\vec{r}_i$, $(i=1,N)$. The associated motion may consist of a rotation around an arbitrary axis through the center of mass depicted by a rotational matrix Ω and a displacement by a translational vector $\vec{R}$. In order to evaluate the coherent dynamic structure factor, we have to generalize the scattering amplitudes of Eq. (5) now describing the object in the initial [1] and final [2] states

$$A_1(Q)=\sum_i b_i e^{i\vec{Q}\cdot\vec{r}_i}, \quad (17a)$$

$$A_2(Q)=\sum_j b_j e^{i\vec{Q}\cdot(\Omega\vec{r}_j+\vec{R})}, \quad (17b)$$

where we explicitly have to include the different scattering lengths into the expression for $S(Q,t)$.

Again performing an isotropic average and for simplicity assuming $b_i=b_j$ for all i and j and removing the scattering length we obtain

$$S(Q,t)=\left[\frac{1}{2}+\frac{1}{N}\sum_{i<j}\frac{\sin(Q|\vec{r}_i-\vec{r}_j|)}{Q|\vec{r}_i-\vec{r}_j|}+\frac{1}{2N}\sum_i\frac{\sin(Q|\vec{r}_i-\Omega\vec{r}_i+\vec{R}|)}{Q|\vec{r}_i-\Omega\vec{r}_i+\vec{R}|}+\frac{1}{N}\sum_{i<j}\frac{\sin(Q|\vec{r}_i-\Omega\vec{r}_j+\vec{R}|)}{Q|\vec{r}_i-\Omega\vec{r}_j+\vec{R}|}\right]+\left[\frac{1}{2}+\frac{1}{N}\sum_{i<j}\frac{\sin(Q|\vec{r}_i-\vec{r}_j|)}{Q|\vec{r}_i-\vec{r}_j|}-\frac{1}{2N}\sum_i\frac{\sin(Q|\vec{r}_i-\Omega\vec{r}_i+\vec{R}|)}{Q|\vec{r}_i-\Omega\vec{r}_i+\vec{R}|}-\frac{1}{N}\sum_{i<j}\frac{\sin(Q|\vec{r}_i-\Omega\vec{r}_j+\vec{R}|)}{Q|\vec{r}_i-\Omega\vec{r}_j+\vec{R}|}\right]e^{-2t/\tau}. \quad (18)$$

As above, the limits $t=0$ and $t=\infty$ reveal the form factor of the rigid object and that of the object occupying both positions simultaneously.

Up to now we have been dealing with coherent scattering from an isolated ensemble of atoms jumping between two equilibrium positions. If such an object is embedded into a matrix with the same average scattering properties as the

considered jumping unit, then the scattering contrast from the average size of the object is matched by the matrix and the corresponding forward scattering is suppressed. Thus, we have to appropriately subtract this scattering intensity from Eq. (18) for $S(Q,t)$.

In order to understand the principle, we consider an ensemble of dumbbells containing two atoms at a fixed distance L. Related to its center of mass $\vec{R}_i$, the ''i'' dumbbell atoms have the coordinates

$$\vec{r}_{i1}=\vec{R}_i+\frac{1}{2}\,\vec{e}_i L, \tag{19a}$$

$$\vec{r}_{i2}=\vec{R}_i-\frac{1}{2}\,\vec{e}_i L, \tag{19b}$$

where $\vec{e}_i$ is a unit vector in the direction of the distance vector between the two atoms. The static structure factor for such an ensemble is given by

$$S(Q)=\frac{1}{N}\left\langle \sum_{\substack{i,j\\ \delta,\gamma}} e^{i\vec{Q}\cdot(\vec{r}_{i\delta}-\vec{r}_{j\gamma})}\right\rangle. \tag{20}$$

Introducing center of mass coordinates [Eq. (19)], $S(Q)$ can be rewritten as

$$S(Q)=\left(1+\frac{\sin(QL)}{QL}\right)+\frac{2}{N}\left\langle \sum_{i<j} e^{i\vec{Q}\cdot(\vec{R}_i-\vec{R}_j)} \times\cos\left(\frac{1}{2}\,\vec{Q}\cdot\vec{e}_i L\right)\cos\left(\frac{1}{2}\,\vec{Q}\cdot\vec{e}_j L\right)\right\rangle. \tag{21}$$

The first part of Eq. (21) represents the orientationally averaged form factor of the dumbbell $\langle A^2(Q)\rangle$. The second part contains the center of mass correlations including correlations between dumbbell orientations and center of mass distances. If we neglect these translational-rotational correlations, the statistical average in Eq. (21) can be split into an orientational and translational one.

$$\begin{aligned}S(Q)&=\langle A^2(Q)\rangle+\frac{2}{N}\left\langle \sum_{i<j} e^{i\vec{Q}\cdot(\vec{R}_i-\vec{R}_j)}\right\rangle\left\langle \cos\left(\frac{1}{2}\,\vec{Q}\cdot\vec{e}_i L\right)\right.\\ &\quad\left.\times\cos\left(\frac{1}{2}\,\vec{Q}\cdot\vec{e}_j L\right)\right\rangle\\ &=\langle A^2(Q)\rangle+\langle A(Q)\rangle^2[S_c(Q)-1],\end{aligned} \tag{22}$$

with $\langle A(Q)\rangle^2=\langle\cos(\frac{1}{2}\vec{Q}\cdot\vec{e}_1 L)\cos(\frac{1}{2}\vec{Q}\cdot\vec{e}_2 L)\rangle_{\Omega_1\Omega_2}$, where the average has to be taken over the orientational configuration spaces Ω_1 and Ω_2. $\langle A(Q)\rangle^2$ is the square of the average scattering amplitude of the dumbbell taken in the center of mass coordinates and $S_c(Q)$ is the structure factor due to the center of mass correlations. Equation (22) can easily be generalized to ensembles of more complicated jumping units. The above reasoning on the structure factor shows, that from the form factor of the jumping unit one has to subtract the square of the average scattering amplitude of the unit $\langle A(Q)\rangle^2$. In this way the forward scattering of the building block is extinguished. This may be considered as subtracting the scattering from the hole in the embedding medium which arises from embedding an object with a form factor $\langle A^2(Q)\rangle$.

Now relating to the dynamic structure factor we commence from Eq. (7b) and obtain for an object embedded in a matrix which performs jumps in a two level system

$$\begin{aligned}S(Q,t)&=\langle[A_1(Q)+A_2(Q)]^2\rangle-\langle A(Q)\rangle^2+\langle A(Q)\rangle^2 S_c(Q)\\ &\quad+\langle[A_1(Q)-A_2(Q)]^2\rangle e^{-2t/\tau}.\end{aligned} \tag{23}$$

For reorientational motions the hole in the embedding medium is not changing and Eq. (23) is valid for arbitrary reorientations. In the case of translational jumps the quantity $\langle[A_1(Q)+A_2(Q)]^2\rangle-\langle A(Q)\rangle^2$ representing the structure factor for $t\to\infty$ may formally lead to negative intensity—if the separation between the initial and final state are sufficiently large $\langle[A_1(Q)+A_2(Q)]^2\rangle$ may decay faster with Q than $\langle A(Q)\rangle^2$. In this case the requirement of overall positive intensity has to be fulfilled by the center of mass correlation term $\langle A(Q)\rangle^2 S_c(Q)$, restricting possible translational jumps to those which are compatible with the translational correlations in the system.

B. Coherent structure factor for two different statistically independent processes

The self-correlation function corresponding to an atom undergoing two different statistically independent processes α and β, can be written as a convolution product of the corresponding self-correlation functions

$$G_s^{\alpha\beta}(\vec{r},t)=\int G_s^{\beta}(\vec{r}',t)G_s^{\alpha}(\vec{r}-\vec{r}',t)d\vec{r}'. \tag{24}$$

This implies that the self- (incoherent) structure factor, which is given by the Fourier transformation of $G_s^{\alpha\beta}(\vec{r},t)$, reads as the direct product of the structure factors corresponding to the two processes

$$S_s^{\alpha\beta}(\vec{Q},t)=S_s^{\alpha}(\vec{Q},t)S_s^{\beta}(\vec{Q},t). \tag{25}$$

However, in the coherent case the derivation of a similar expression is not straightforward, because the correlations between all the pairs of scatters (j,i) have to be taken into account. The coherent structure factor for the α-β process can be written in a general form as

$$S^{\alpha\beta}(\vec{Q},t)=\frac{1}{N}\sum_j\sum_i \Phi_{ji}^{\alpha\beta}(\vec{Q},t), \tag{26}$$

where $\Phi_{ji}^{\alpha\beta}(\vec{Q},t)$ is the correlation function corresponding to the pair (j,i) and N the number of particles. Expression (26) can also be written as

$$S^{\alpha\beta}(\vec{Q},t)=\frac{1}{N}\sum_j\sum_i \Phi_{ji}^{\alpha\beta}(\vec{Q})\varphi_{ji}^{\alpha\beta}(\vec{Q},t), \tag{27}$$

where now $\varphi_{ji}^{\alpha\beta}(\vec{Q},t)$ is a correlation function normalized to 1 at $t=0$. If α and β are considered statistically independent processes, $\varphi_{ji}^{\alpha\beta}(\vec{Q},t)=\varphi_{ji}^{\alpha}(\vec{Q},t)\varphi_{ji}^{\beta}(\vec{Q},t)$ and Eq. (27) becomes

$$S^{\alpha\beta}(\vec{Q},t)=\frac{1}{N}\sum_j\sum_i \Phi_{ji}^{\alpha\beta}(\vec{Q})\varphi_{ji}^{\alpha}(\vec{Q},t)\varphi_{ji}^{\beta}(\vec{Q},t), \quad (28)$$

which using the Vineyard approximation [15] for the α process can be expressed as

$$S^{\alpha\beta}(Q,t)=S_s^{\alpha}(Q,t)S^{\beta}(Q,t), \quad (29)$$

where $S^{\beta}(\vec{Q},t)=(1/N)\Sigma_j\Sigma_i\Phi_{ji}^{\alpha\beta}(\vec{Q})\varphi_{ji}^{\beta}(\vec{Q},t)$ is the coherent structure factor of the β process. In this framework we obtain an expression for $S^{\alpha\beta}(\vec{Q},t)$ connecting the coherent structure factor of the β relaxation with the relaxation function of the α process, where in the language of the Vineyard approximation $S^{\beta}(\vec{Q},t)$ takes the role of $S(Q)$.

III. NEUTRON SPIN ECHO STUDY: EXPERIMENT AND RESULTS

A. Sample

The experiments were performed on a perdeuterated PB(—CD_2—CD═CD—CD_2—)$_n$ synthesized by anionic polymerization [16]. Purified *sec*-butyllithium was used as the initiator and benzene as the solvent. The reaction conditions used led to a statistically uniform, stereoirregular chain microstructure of 52% 1,4-*trans*, 41% 1,4-*cis*, and 7% 1,2 (vinyl)-units. Molecular weight and polydispersity were $M_N=31.6\times10^3$ and $M_W/M_N<1.02$ as determined by membrane osmometry in toluene at 310 K and size exclusion chromatography, respectively. With differential scanning calorimetry (DSC) T_g was determined to be 178 K.

B. Neutron spin echo experiments

The NSE experiments were performed by means of the spectrometer IN11 at the Institute Laue Langevin (ILL) in Grenoble. As described elsewhere [14], NSE measures directly the normalized intermediate scattering function $S(Q,t)/S(Q,0)$, where t is the time. Since incoherent scattering contributions are strongly suppressed, the signal from our deuterated PB sample is nearly entirely due to coherent scattering. The experiments were performed at the highest scattering angle available (128°), allowing us to reach a maximum Q value of 2.71 Å^{-1} for the minimum incoming wavelength λ available (4.16 Å). By changing the value of λ we measured spectra at 205 K for different Q values in the range 1.40 Å$^{-1}<Q<$2.71 Å^{-1}, accessing the dynamics around the first and second maxima as well as around the minimum of the static structure factor $S(Q)$ [10]. For several Q values and, in particular, for $Q=2.71$ Å^{-1} we also measured spectra at different temperatures ranging between 170 K and 300 K. The time window varies with Q from 1.8 ps$<t<$1.5 ns ($Q=2.71$ Å^{-1}) to 13 ps$<t<$6.3 ns ($Q=1.40$ Å^{-1}). For each momentum transfer the instrumental resolution function was determined from the elastic scattering of the sample at 4 K. The instrumental background as well as the scattering from the Al container and the cryostat was measured separately and subtracted from the experimental spectra using the appropriate transmission factors. Thereby, the most important background was found at the two highest Q values where the Debye-Scherrer rings of the Al resulted in an elastic background of about 20% of the total signal. The background corrected spectra were divided by the resolution function yielding the normalized intermediate dynamic structure factors $S(Q,t)/S(Q,0)$. In addition, in this work we have reanalyzed previous data reported in Refs. [6] and [7].

C. Neutron spin echo results

In a first approach, we fitted the NSE data with a Kohlrausch-Williams-Watts (KWW) [17] function,

$$\frac{S(Q,t)}{S(Q,0)}\propto\exp\left[-\left(\frac{t}{\tau_{\mathrm{KWW}}}\right)^{\beta}\right], \quad (30)$$

which describes the decay of the density fluctuations through the α relaxation. As will be shown below, the value of the shape parameter β obtained for this process by dielectric spectroscopy is 0.41. Therefore, we fitted NSE data by means of Eq. (30) and $\beta=0.41$, expecting a viscositylike temperature dependence of τ_{KWW} in the case that we are really observing the primary relaxation. The results of scaling the time scale of NSE data with $\tau_\eta\propto\xi(T)/T$, where ξ is the monometric friction coefficient obtained from viscosity measurements [18], are shown in Fig. 2(b) for $Q=1.48$ Å^{-1} and in Fig. 2(c) for $Q=2.71$ Å^{-1}. These two Q values lie close to the first and the second maxima of $S(Q)$, respectively, [see Fig. 2(a)]. As can be seen in Fig. 2(b), the whole master curve obtained for $Q=1.48$ Å^{-1} can be described, within the experimental uncertainties, with a KWW function with $\beta=0.41$. This result is compatible with an earlier result [6], where a β value of 0.45 was obtained from the fitting of the master curve to a KWW function. In contrast for $Q=2.71$ Å^{-1} obviously the spectra do not follow a time temperature superposition principle determined by τ_η and strong deviations from a single master curve are found [see Fig. 2(c)].

Figure 3 evidences the difference between the temperature dependences of the τ_{KWW} obtained for the two Q values in question. For $Q=1.48$ Å^{-1} the characteristic time scale can be perfectly fitted by $\tau_{\mathrm{KWW}}\propto\xi(T)/T$, as we could expect from Fig. 2(b), whereas for $Q=2.71$ Å^{-1} the characteristic times follow clearly an Arrhenius-like temperature dependence. The fitted line in Fig. 3 for $\tau_{\mathrm{KWW}}(Q=2.71$ Å$^{-1})$ corresponds to $\tau_{\mathrm{KWW}}=\tau_{\mathrm{KWW}_0}^{\mathrm{NSE}}\exp(E_0/kT)$ with $\tau_{\mathrm{KWW}_0}^{\mathrm{NSE}}=1.9\times10^{-18}$ s and $E_0=0.40$ eV. The observed activation energy agrees perfectly with that found for the dielectric β relaxation (see below). We would like to point out that the KWW function used in our description of the data also describes approximately the relaxation function corresponding to the dielectric β relaxation in the time domain if we restrict the time range to the NSE window. From this simple analysis we conclude that around the first maximum of $S(Q)$, which is governed by interchain correlations [10], the dynamics are clearly related to the α relaxation, whereas around the second maximum, which reflects intrachain correlations [10], the dynamics are connected to the β relaxation.

These results, together with the observation of the decoupling of the characteristic time scale from the viscosity towards the β relaxationlike behavior in the minimum of $S(Q)$ [7], clearly show that the β process contributes to the dynamic structure factor in the NSE window.

Below T_M ($\approx$210 K) the α relaxation slows down very

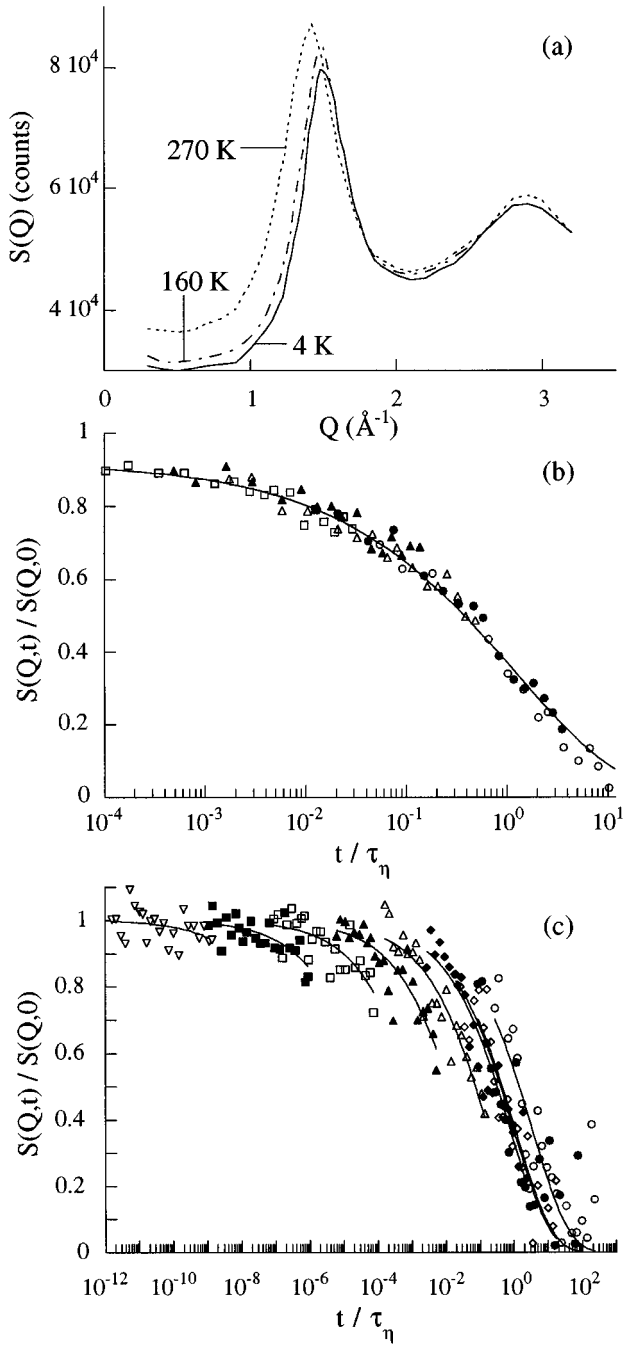

FIG. 2. (a) Static structure factor obtained by *D*1*B* (ILL) for deuterated PB at different temperatures (extracted from Ref. [10]). (b) Scaling representation of the NSE data at 1.48 Å^{-1} (○ 280 K; ● 260 K; △ 240 K; ▲ 230 K; □ 220 K); (c) the same kind of representation for 2.71 Å^{-1} (○ 300 K; ● 280 K; ◇ 260 K; ◆ 240 K; △ 220 K; ▲ 205 K; □ 190 K; ■ 180 K; ▽ 170 K). Solid lines correspond to KWW functions (see text).

rapidly with decreasing temperature and cannot be observed anymore within the window of NSE. Therefore, the analysis of the structure factor has been performed distinguishing two dynamical regimes: the β regime, at $T<T_M$, where we measure the β process, and the α-β regime at $T>T_M$, where in principle both, the β and the α process could be present in NSE window.

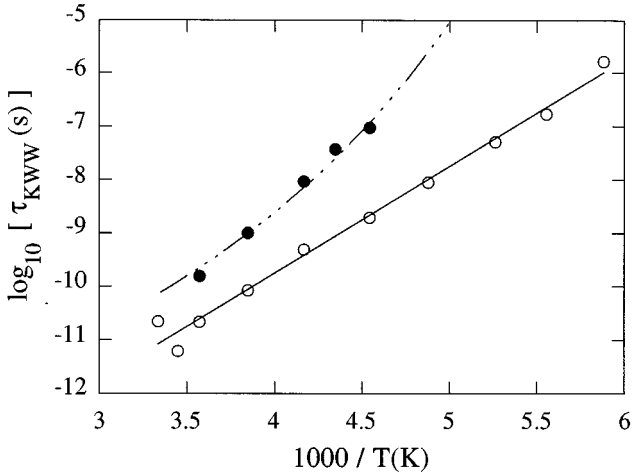

FIG. 3. Temperature dependence of the characteristic times τ_{KWW} obtained from the fits of $S(Q,t)$ to stretched exponentials with $\beta=0.41$ at $Q=1.48$ Å^{-1} (●) and 2.71 Å^{-1} (○). Dashed-dotted line corresponds to the Vogel-Fulcher-like temperature dependence of the viscosity for $Q=1.48$ Å^{-1} and the solid line to the Arrhenius-like temperature dependence of the dielectric β relaxation for $Q=2.71$ Å^{-1}.

IV. NEUTRON SPIN ECHO STUDY: EVALUATION IN THE β REGIME

The β relaxation is generally assumed to be a spatially localized process; e.g., results from dielectric spectroscopy are commonly interpreted in terms of distributions of elemental local jump processes [1]. The simplest picture of such a process is a jump of an atom between two equivalent sites separated by a distance d with a characteristic time $\tau=\tau_0^{\mathrm{NSE}}\exp(E/kT)$. Scattering functions for incoherent and coherent scattering for these two level jump processes were discussed in Sec. II. As we have seen, coherent and incoherent scattering differ with respect to the presence of interference terms in the coherent scattering. For uncorrelated motion dynamic constructive interferences are absent [Eq. (12)] and it follows naturally that the coherent quasielastic part assumes the form of the incoherent structure factor [Eq. (4)]. Note that the interference terms from the average atom distribution remain giving rise to $S(Q)$. If the motions are correlated we have shown above that the interference effects are small as long as the jump distances are smaller than the distance between the atom pairs.

In a first approach to model the β relaxation we thus approximate the coherent quasielastic form factor by the incoherent one. Then with Eq. (4) the normalized dynamic structure factor may be written as

$$\frac{S(Q,t)}{S(Q)}=1-\frac{1}{2S(Q)}\left[1-\frac{\sin(Qd)}{Qd}\right]+\frac{1}{2S(Q)}\left[1-\frac{\sin(Qd)}{Qd}\right]e^{-2t/\tau} \tag{31a}$$

$$=1-\frac{F^{\mathrm{el}}(Q,d)}{S(Q)}+\frac{F^{\mathrm{inel}}(Q,d)}{S(Q)}\,e^{-2t/\tau}. \tag{31b}$$

As mentioned above the secondary relaxation cannot be described by means of a single Debye process, but more

complicated relaxation functions involving distributions of relaxation times, like the Cole-Cole function [19], or distributions of energy barriers, like log-normal functions [20], have to be used for its description. We mention here in advance that the dielectric β-relaxation function of PB can be well described by assuming a superposition of Debye elemental processes with a Gaussian distribution of energy barriers $g(E)$,

$$\varphi_\beta(t)=\int_0^\infty g(E)\exp\left[-\frac{t}{\tau_0^D\exp\left(\frac{E}{kT}\right)}\right]dE, \qquad (32a)$$

$$g(E)=\frac{1}{\sqrt{\pi}\sigma}\exp\left[-\left(\frac{E-E_0}{\sigma}\right)^2\right]. \qquad (32b)$$

Here σ is the width and E_0 is the average of the distribution of activation energies. The width σ decreases linearly with temperature $[\sigma(\mathrm{eV})=0.145-2.55\times10^{-4}\,T(K)]$. The narrowing of the relaxation function with increasing temperature is another well established feature of the β relaxation [1]. The values of τ_0^D and E_0 are determined from the temperature dependence of the position of the maximum of the relaxation, $\tau_{\max}=\tau_0^D\exp(E_0/kT)$ and they are $\tau_0^D=3.5\times10^{-17}$ s and $E_0=0.41$ eV. The coherent dynamic structure factor corresponding to the β process can now be built by a superposition of the coherent scattering functions for the elemental processes [Eq. (31)] weighted by the Gaussian distribution function of the activation energies $g(E)$

$$\frac{S(Q,t)}{S(Q)}=1-\frac{1}{S(Q)}\int_0^\infty g(E)F^{\mathrm{el}}(Q,d(E))dE + \frac{1}{S(Q)}\int_0^\infty g(E)F^{\mathrm{inel}}(Q,d(E))e^{-2t/\tau(E)}dE. \qquad (33)$$

The free parameters in this model are d and τ_0^{NSE}. For d we choose the dependence on the activation energy given by the soft potential model, i.e., $d\propto E^{1/4}$ [21], giving a slight variation of d in the energy range where $g(E)$ presents significant values. We also allowed a Q and temperature dependent amplitude factor which accounts for fast processes like phonons. The best fit was obtained for $d(\text{Å})=1.9\ E(\mathrm{eV})^{1/4}$ implying a most probable jump distance of 1.5 Å and $\tau_0^{\mathrm{NSE}}=\tau_0^D/250$.

As can be seen from Fig. 4 with this approach we obtain a very good description of all the NSE data at all temperatures and Q values investigated. We would like to emphasize the astonishing result that the time scale observed for the relaxation of density fluctuations by NSE is shifted by approximately two orders of magnitude to shorter times with respect to the time scale observed for dipole relaxation. Recent light scattering experiments on the β relaxation of 1,4 PB also suggest a similar shift of the observed time scale compared to that of dielectric relaxation [22]. A difference of one decade for a given temperature between the time scale obtained from dielectric relaxation compared to that of NSE at $Q=1.88$ Å^{-1} [7] is reported in [23]. However, in that work a PB sample with a different microstructure [20% (vinyl) units] was investigated. As shown by Hofmann *et al.* [12], the β relaxation in samples with intermediate microstructure between 1,4 PB and 1,2 PB behave differently from the β relaxations in the two borderline microstructures, being apparently even faster than in 1,4 PB for certain contents of vinyl groups.

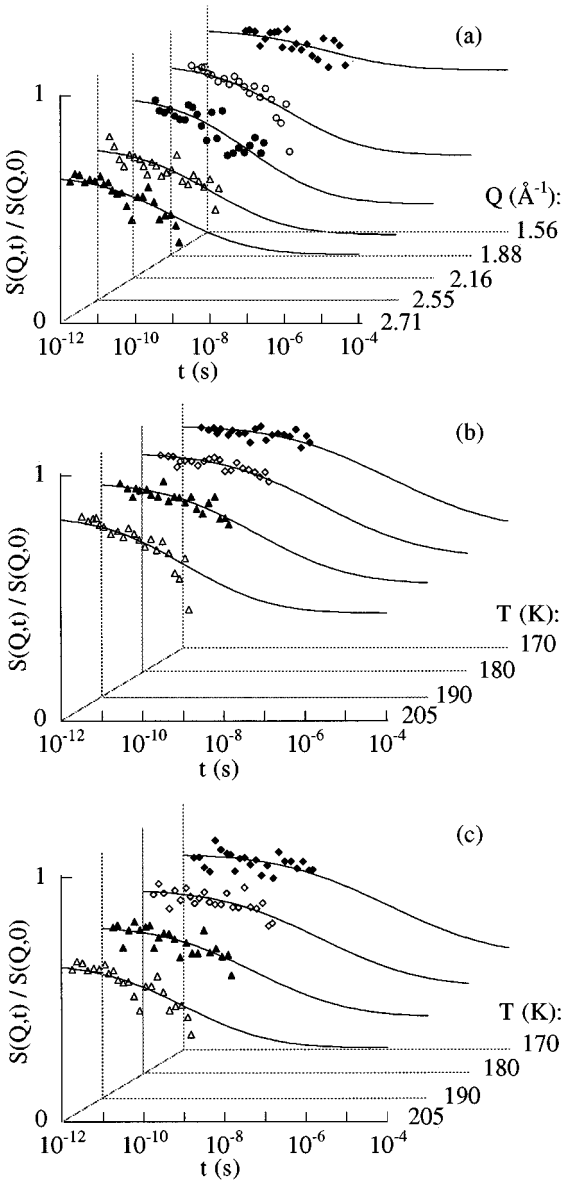

FIG. 4. NSE spectra at 205 K (a) for the Q values indicated; at $Q=1.88$ Å^{-1} (b) and 2.71 Å^{-1} (c) for the temperatures indicated. Solid lines are the fitting curves obtained in the incoherent approximation for the inelastic part [9].

This simple description of the dynamic structure factor for the β relaxation immediately explains the qualitatively different behavior of $S(Q,t)$ at the two first maxima of $S(Q)$. Figure 5(a) displays the relative quasielastic contribution of the β process $F^{\mathrm{inel}}(Q)$ to the normalized dynamic structure factor as calculated on the basis of the parameter obtained through the fitting procedure described above (solid line). This contribution is very small in the neighborhood of the first peak, so there at higher temperatures we are mainly

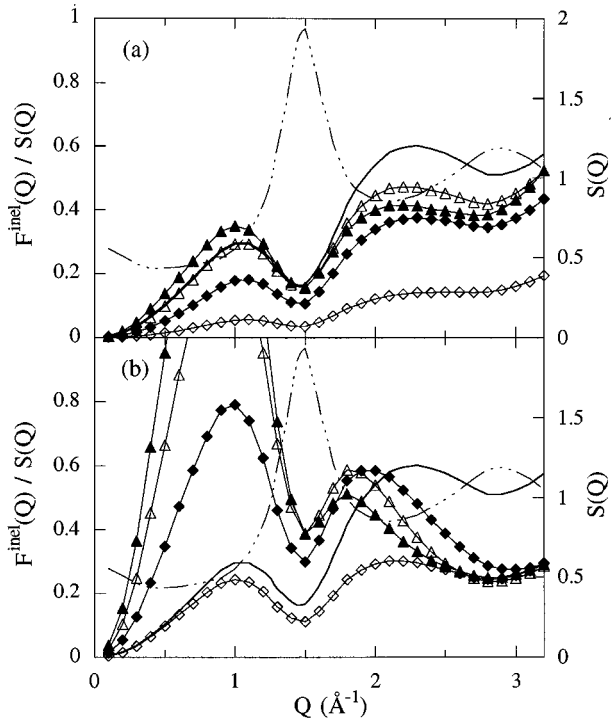

FIG. 5. Q dependence of the amplitude of the relative quasielastic contribution of the β process to the coherent scattering function obtained in the incoherent approximation for the inelastic part (solid line) and from the cis unit rotation model for the rotation axis through the center of mass of the unit (a) and through the main chain (b) for different angles: 30° (◇), 60° (◆), 90° (△), and 120° (▲). The static structure factor $S(Q)$ at 160 K [10] is shown for comparison (dashed-dotted line).

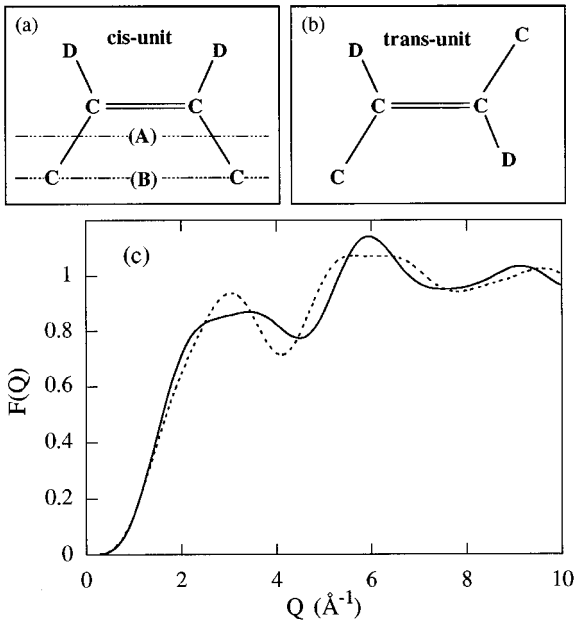

FIG. 6. Schematic representation of cis (a) and trans (b) units and the form factors associated to them (c): solid line corresponds to cis unit and dotted line to trans unit. The form factors $F(Q)$ displayed correspond to $F(Q)=\langle A(Q)^2\rangle-\langle A(Q)\rangle^2$ [Eq. (22)], where $A(Q)a$ are the scattering amplitudes of the *cis* or *trans* group. The positions of the rotation axes considered for the cis unit are shown in (a): axis through the center of mass (A) and through the main chain (B).

observing the contribution of the α relaxation. On the other hand, $F^{\text{inel}}(Q)$ is quite high around the minimum and the second peak of $S(Q)$, explaining the Arrhenius behavior of the characteristic times of Fig. 3 at $Q=2.71$ Å^{-1} and the decoupling observed at $Q=1.88$ Å^{-1} [7].

Up to now we have considered the dynamic structure factor in incoherent approximation which, as we have shown in Sec. II, may be a reasonable approximation under certain conditions. Now we would like to approach the molecular geometry more closely, and consider, in an exemplary way, possible motions of the building blocks of PB. Examining the molecular structure we realize that the polymer is built from basically two different rigid units, the *cis* and the *trans* units, comprising each four carbon and two deuterium atoms (Fig. 6). Both are of similar geometry and mainly distinguish themselves in the way the polymer backbone continues. These two building blocks are randomly incorporated into the chain backbone and are connected by one CD_2 unit, respectively. In order to model the local dynamics properly we would have to treat the local chain structure using, e.g., the rotational isomeric state approach [24], to couple the chain to the surrounding other chains, to formulate proper rate equations and to calculate $S(Q,t)$ on this basis. Such a calculation goes far beyond this work and will be followed in the future. Here we like to go only one step beyond the incoherent approximation and investigate the changes of $S(Q,t)$, if we take into account rigid jumping units as discussed in Sec. II [Eq. (18) and (23)]. Since the form factors of the *cis* and *trans* units are rather similar (Fig. 6) we treat only motions of the *cis*-group expecting similar results also for the *trans* unit. We note, that the *cis* group carries the dielectric dipole. Therefore, its motion is observed by dielectric spectroscopy.

Both units exhibit form factors showing a first intensity maximum around $Q=3$ Å^{-1} and a second maximum around 6 Å^{-1} before the intensity approaches the asymptotic value of 1. Note that at ≈ 3 Å^{-1} we experimentally see a high contribution of the β process to the structure factor. With this in mind, we consider as a possible elemental process the rotation of a *cis* unit around a given axis parallel to the double bond and on the plane defined by the C—CD═CD—C rigid unit (see Fig. 6). We have calculated the form factor associated with this motion. On the basis of Eqs. (18) and (23) we have calculated $F^{\text{inel}}(Q)$ for different angles of rotation around an axis passing through the center of mass of the unit in Fig. 5(a) and through the extremal C atoms in Fig. 5(b). Considering first the rotation around the center of mass axis, we realize that the coherent inelastic form factors for the *cis* unit performing rotational jumps of different angles follow qualitatively the result of the incoherent approximation for 1.5 Å jumps. Thereby rotational angles between 60° and 120° are, in particular, close to Eq. (33) indicating that rotational jump processes of this order are clearly compatible with the observed NSE spectra. The picture is quite different for rotations around the axis through the extremal C atoms of the *cis* unit. In this case strong inelastic scattering is predicted to occur around 1 Å^{-1}. For

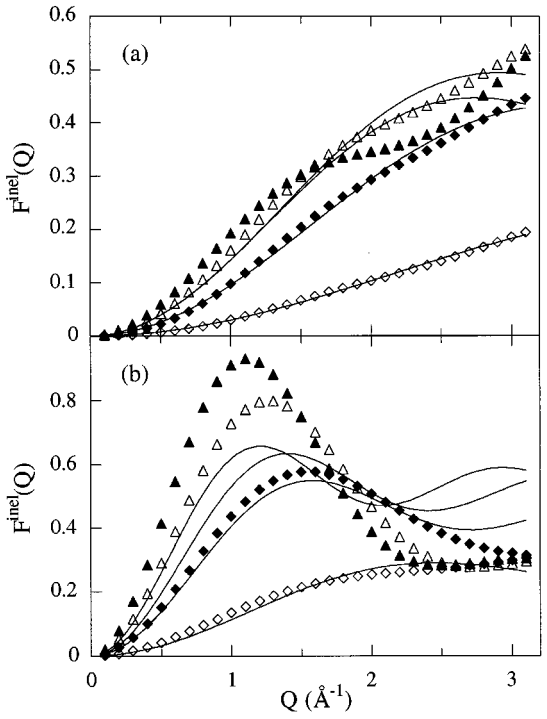

FIG. 7. Inelastic contribution of the β process to the scattering function obtained from the cis unit rotation model for the rotation axis through the center of mass of the unit (a) and through the main chain (b) for different angles: 30° (◇), 60° (◆), 90° (△), and 120° (▲). Solid lines correspond to fitting curves to Eq. (34).

rotational angles >70° the consistency condition of Eq. (23) cannot be fulfilled leading to negative elastic intensities. Thus, such angles are forbidden. The inelastic contribution to the coherent scattering function [Eq. (23)] for the rotations considered in Fig. 5 is shown in Fig. 7. Here we have fitted these functions to the expression

$$F^{\mathrm{inel}}(Q) \propto \frac{1}{2}\left[1-\frac{\sin(Qd_{\mathrm{eff}})}{Qd_{\mathrm{eff}}}\right], \tag{34}$$

i.e., to the functional form of the incoherent approximation. The fits are reasonable for the rotations around the center of mass [values for the effective distance d_{eff} obtained: 0.98 Å (30°); 1.33 Å (60°); 1.54 Å (90°); 1.64 Å (120°)]. This result also indicates that the earlier results from the incoherent approximation are in best agreement with rotational jumps between 60° and 90° around this axis. On the other hand, we observe from Fig. 7(b) that the agreement with Eq. (34) is not good for rotations of high angles around the main chain, which would involve much larger distances [d_{eff}: 1.84 Å (30°); 2.85 Å (60°); 3.21 Å (90°); 3.71 Å (120°)].

We conclude that the NSE data are compatible with rotational processes of the rigid building blocks of PB around an axis passing through their center of mass. Rotations around an axis along the main chain atoms at the extremities lead to intensity at too low Q and are not likely. Thus, such rotational processes around the center of mass axis are likely to be the motional mechanism behind the β relaxation. We note, however, that the experimentally observed Q dependences lead to more pronounced sharper structures around $Q \approx 3$ Å^{-1} indicating that the scattering in this Q region may contain interference terms from several building blocks along the chain. Thus reorientational motions involving cooperatively more than one building block are likely. Since a description in terms of simple hopping [Eq. (34)] appears to be a good approximation to this more realistic picture and since the corresponding equations are much easier to handle, we shall use these expressions in the following.

V. NEUTRON SPIN ECHO STUDY: EVALUATION IN THE α-β REGIME

At temperatures in the order of the merging temperature T_M the characteristic relaxation times of the primary α relaxation reaches similar orders of magnitude as that of the local β relaxation. Therefore the description of the dynamic structure factor will have to be generalized also including the segmental diffusion process underlying the α process. We have considered and successfully described the β process as a local intrachain relaxation process which takes place within the fixed environment set by the other chains. When the segmental diffusion reaches the time scale of the local relaxation, given atoms and molecular groups will noticeably participate, simultaneously, in both motional mechanisms: the intrachain β relaxation and the interchain α relaxation. We now start with the hypothesis that to first order both mechanisms are statistically independent from each other. We shall see that on the basis of this hypothesis the Q and temperature dependent dynamic structure factors in the merging regime and above can be consistently accounted for.

As shown in Sec. II under the assumption of statistical independence of α and β processes and a Vineyard approximation for the α process the coherent dynamic structure factor $S^{\alpha\beta}(Q,t)$ can be expressed by Eq. (29). Following common wisdom we describe the relaxation function for the α process by a KWW function

$$\varphi^{\alpha}(Q,t)=\exp\left\{-\left[\frac{t}{\tau_{\mathrm{KWW}}(Q,T)}\right]^{\beta}\right\}, \tag{35}$$

with β=0.41 from the shape of the dielectric spectra. $\tau_{\mathrm{KWW}}(Q,T)$ is the characteristic Q and temperature dependent relaxation time. For the β process we take the structure factor given by Eq. (33) leading to

$$\begin{aligned}\frac{S^{\alpha\beta}(Q,t)}{S(Q)}=&\exp\left\{-\left[\frac{t}{\tau_{\mathrm{KWW}}(Q,T)}\right]^{\beta}\right\}\\ &\times\left[1-\frac{1}{S(Q)}\int_0^{\infty}g(E)F^{\mathrm{el}}(Q,d(E))dE\right.\\ &\left.+\frac{1}{S(Q)}\int_0^{\infty}g(E)F^{\mathrm{inel}}(Q,d(E))e^{-2t/\tau(E)}dE\right].\end{aligned} \tag{36}$$

Note that all the parameters involved in the coherent structure factor of the β relaxation are known from the evaluation described above. They are extrapolated to the higher temperatures. The only free parameters in fitting the NSE data to Eq. (36) are: (i) a Q and temperature dependent amplitude factor which accounts for fast processes like

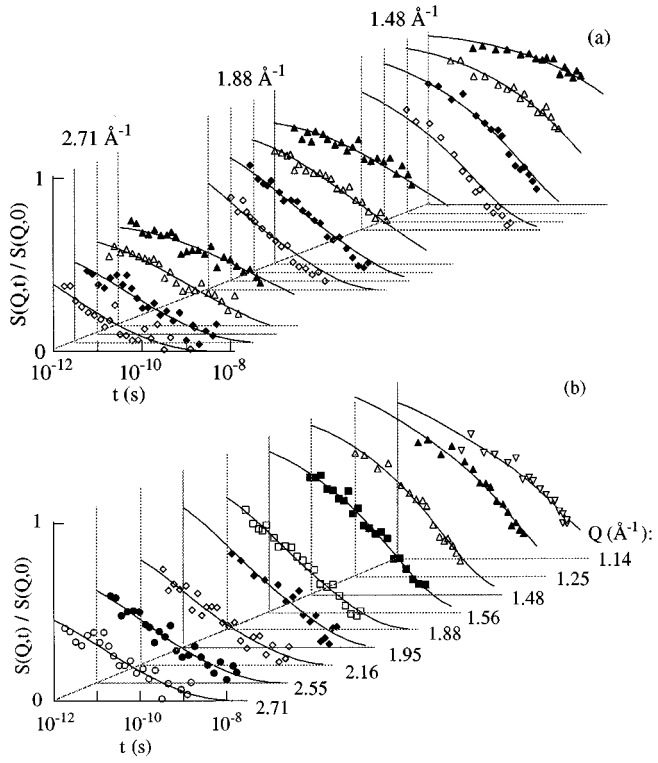

FIG. 8. (a) NSE spectra for the Q values indicated at 220 K (▲), 240 K (△), 260 K (◆), and 280 K (◇). (b) at 260 K for the Q values indicated. Solid lines are fitting curves (see text).

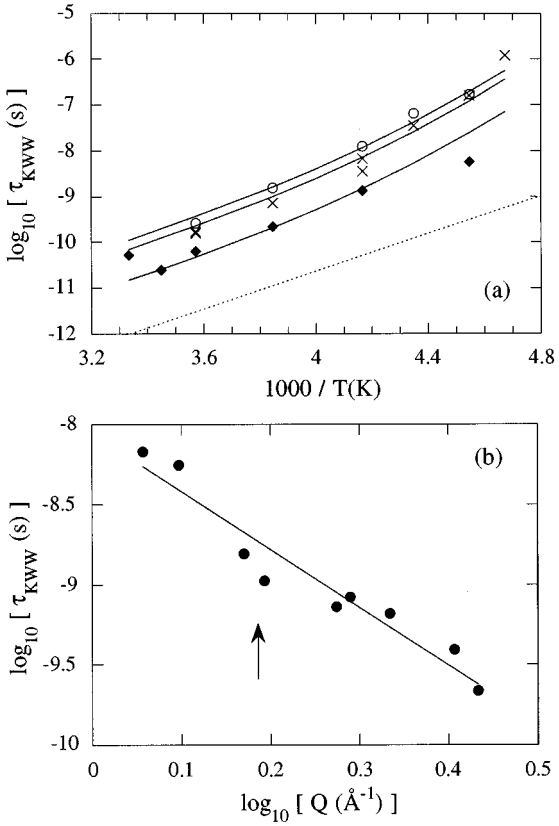

FIG. 9. (a) Temperature dependence of the characteristic times of the α relaxation τ_{KWW} for $Q=1.48$ Å^{-1} (○), 1.88 Å^{-1} (×), and 2.71 Å^{-1} (◆). Solid lines show the temperature dependence of the viscosity. The time scale (maximum of the distribution) of the β relaxation is also shown for comparison (dashed line). (b) Q dependence of τ_{KWW} at 260 K. The solid line corresponds to the fit to Eq. (37).

phonons and (ii) the characteristic time of the α relaxation τ_{KWW} which depends on both Q and temperature. The temperature dependence of τ_{KWW} should follow the viscosity relaxation and can be also fixed to the viscosity temperature scale, i.e., $\tau_{KWW}(Q,t)=B(Q)\zeta(T)/T$; the Q-dependent proportionality factor $B(Q)$ is then the free parameter. Figure 8 shows resulting fitting curves for several temperatures at the first maximum, minimum and second maximum of $S(Q)$ [Fig. 8(a)] and for 260 K at different Q values [Fig. 8(b)]. The excellent agreement between the scattering function [Eq. (36)] and the experiment strongly supports the hypothesis that the α and β relaxations behave independently of each other.

It is noteworthy to remark that in the fitted structure factor shown in Fig. 8 all the parameters are fixed except an amplitude factor and the Q dependence of $\tau_{KWW}(Q,T)$. The small deviations of the curves at 280 K for 1.48 Å^{-1} and 1.88 Å^{-1} could be related to a possible small increase of the shape parameter β at high temperatures.

The different amplitude factors result from fast relaxations and soft phonons which contribute to $S(Q,t)$ outside the observation window but inside the bandpass of IN11. If such processes amount to an important fraction of the total scattering within the bandpass, then they are accounted for in the normalization process leading to the echo amplitude. But since they are too fast to be observable directly within the instrumental time window, they just reduce the apparent NSE amplitude. Time of flight (TOF) experiments which reach to shorter times may be used, to determine these amplitudes from measured spectra. Using coherent spectra which were measured on the same sample at the cold TOF spectrometer IN6 [25] we extracted the fast inelastic fraction of corresponding spectra at $Q=1.48$ Å^{-1} and $Q=1.88$ Å^{-1} within the 5 meV bandpass of IN11. These amplitude factors could approximately be described by $\exp[-f(Q)T]$, and agreed well with the fitted amplitudes. Using the thus determined amplitudes we refitted varying now both the Q and temperature dependence of $\tau_{KWW}(Q,T)$. The temperature dependence of the resulting values of $\tau_{KWW}(Q,T)$ is shown in Fig. 9(a) for 1.48 Å^{-1}, 1.88 Å^{-1}, and 2.71 Å^{-1}. The agreement with the viscosity temperature scale shown by the solid lines is generally very good. In the case of 2.71 Å^{-1} where IN6 data are not available a DWF-like temperature dependence of the amplitudes was assumed. This could be the reason for the slight deviation at 220 K. As can be seen in Fig. 8, this spectrum is very well represented by the theoretical curve if the time scale is fixed to follow the viscosity temperature dependence and the amplitude is the free parameter. The Q dependence of the τ_{KWW} is shown by Fig. 9(b) where the results for all the Q available at 260 K are displayed. The fit to a power law

$$\tau_{KWW}(Q,T)\propto Q^{-n} \tag{37}$$

gives an n value of $n=3.62$. In coherent scattering from a diffusive process we would expect to observe ''de Gennes

narrowing'' [26] of the quasielastic line, i.e., a modulation of the characteristic time with the static structure factor. We like to point out that the data on $\tau_{KWW}(Q)$ do not evidence any clear modulation with $S(Q)$. If anything, in the region of the first peak of $S(Q)$ [arrow in Fig.9(b)], the $\tau_{KWW}(Q)$ values are below and not above the solid line dictated by the power law. This result supports the consistency of the used Vineyard approximation for the α process which is based on the incoherent dynamic structure factor. Here we find practically the same power law as observed in earlier incoherent scattering studies [27,25]. Moreover, the ''de Gennes narrowing'' has only been established in a straightforward way for monoatomic liquids [26]. Which modifications would be necessary in order to describe a complex polymer liquid is not known.

In conclusion within the experimental accuracy the coherent Q-dependent dynamic structure factor in the α-β relaxation regime of 1,4 PB can be consistently described under the assumption that both processes are statistically independent. This observation based on the Q and temperature dependence of $S^{\alpha\beta}(Q,t)$ opens also an approach for an understanding of results from dielectric spectroscopy on polymers. This will be dealt with in the next sections.

VI. DIELECTRIC STUDY: EXPERIMENT AND RESULTS

A. Dielectric experiments

Dielectric measurements were carried out between 10^{-2} to 10^9 Hz by combining three different measurement systems: (i) the range 10^{-2} to 10^6 Hz was covered with a frequency response analyzer Schlumberger 1260 equipped with a Chelsey dielectric interface with high impedance preamplifier; (ii) a Hewlett-Packard impedance analyzer 4192 A allowed us to measure the dielectric response in the audio frequency range (10^3 to 10^7 Hz) and (iii) the range between 10^6 to 10^9 Hz was investigated by using a Hewlett-Packard impedance analyzer 4191 A, which is based on the principle of a reflectometer.

The sample holder used in the case of systems (i) and (ii) consisted of a parallel-plate capacitor (diameter 20 mm). By the measurements with (iii) the sample was kept between two gold-plated stainless steel electrodes (diameter 6 mm). The distance between the plates and electrodes (50 μ) could be kept constant by insertion of small Teflon spacers. Because the distance could not be determined to higher accuracy than 10%, this is also the minimum error of the absolute value of the dielectric constant and loss.

The measurements were performed on the same sample as NSE experiments. From the three different monomeric units present in the sample (1,4-*cis*, 1,4-*trans*, and 1,2-vinyl), unit 1,4-*trans* has no dipole moment (*trans*-2-butene) whereas the others have a dipole moment of the same order of magnitude: 0.33 Debye (*cis*-2-butene) and 0.5 Debye (Methylpropene) [28]. Therefore, taking into account that the number of vinyl groups in our sample is much lower than the number of *cis* units, the dielectric response is mainly due to the 1,4-*cis* groups. On the other hand, the sample was so clean that no additional dc-conductivity contribution at the low frequency side had to be taken into account.

All measurements were done under isothermal conditions with a temperature stability better than 0.1 K. The temperature range investigated was 125 K$<T<$260 K. Between 125 K and 170 K the spectra were measured each 2.5 K; in the temperature region 170 K$<T<$182 K, each 1 K, and for $T>$182 K, each 2 K. Due to the low value of the dipole moment of the sample, with the HP 4191 A it was possible to resolve the dielectric response only at high temperature, where the maximum of the loss occurs at frequencies close to its frequency window.

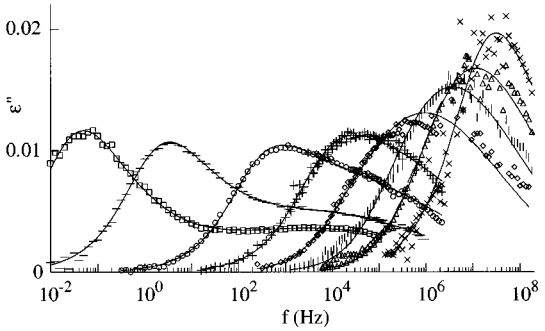

FIG. 10. Dielectric loss curves obtained for PB at 175 K (□), 180 K (−), 190 K (○), 200 K (+), 210 K (◇), 220 K (|), 230 K (△), and 240 K (×). Solid lines through the points are the corresponding fitting curves (see text).

B. Dielectric results

The dielectric loss curves obtained for PB show the commonly observed behavior on amorphous polymers: at temperatures below T_g only one relaxation process, the β relaxation, is active in the dielectric frequency window, whereas above T_g the contribution of the α relaxation is also measured. As can be seen in Fig. 10, two loss processes approaching each other with increasing temperature can be distinguished in a narrow temperature range above T_g, the α relaxation taking place at lower frequencies than the β relaxation. At high temperatures ($\approx T_g+30$ K) α and β relaxations merge and only one peak can be resolved in the experimental dielectric window.

From a phenomenological point of view, a characteristic time scale can be defined as the inverse of the frequency at

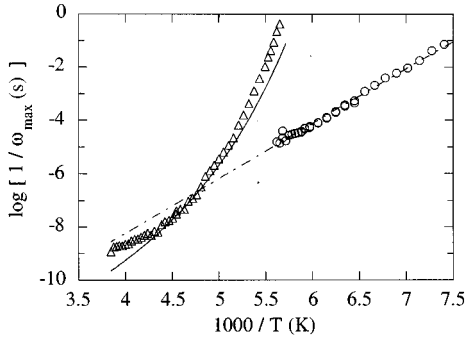

FIG. 11. Temperature dependence of the logarithm ($\log_{10}$) of the characteristic time scales defined as the inverse of the frequencies of the dielectric loss maxima for the main relaxation process (△) and the β relaxation (○). The solid line shows the temperature behavior of the viscosity and the dashed-dotted line the Arrhenius-like dependence of the β relaxation.

which the dielectric loss presents a maximum. Figure 11 shows the temperature dependence of such determined characteristic times of the α and β relaxations in PB. In the region well below the merging these time scales can be univocally determined, but further away from T_g only a change in the slope of the high frequency tail of the dielectric loss evidences the presence of the β relaxation (see Fig. 10). Therefore, in this temperature range only the evolution of one maximum, which should be in principle assigned to the main (α) relaxation, can be followed. Concerning the β relaxation, an Arrhenius-like temperature dependence [3] of the time scale is observed $\tau_{\max}=\tau_0^D \exp(E_0/kT)$ like in many other glass-forming polymeric systems [1]. We can see in Fig. 11 that the extrapolation of this law to high temperature crosses the points corresponding to the experimentally observed maxima. The temperature at which both time scales coincide, around 210 K, can be referred to as the merging temperature T_M. At higher temperatures, the extrapolated values for the time scales corresponding to the maxima of the β relaxation are higher than the values found for the experimental maxima. No signature of such a contribution to the dielectric loss in the low frequency range is observed (see Fig. 10). This would lead us to think that the β process dies out above the merging. On the other hand, the temperature dependence of the characteristic time scale of the main process clearly differs from the temperature behavior of the time scale associated with the viscosity, as can also be seen in Fig. 11.

VII. DIELECTRIC STUDY: THEORETICAL CONSIDERATIONS

Dielectric data are usually analyzed under the assumption that the total dielectric response can be obtained from the addition of the contributions of α and β relaxations. This seems to give a good description of the experimental data when both processes are well separated, i.e., below the merging. However, if one tries to fit the data close or above the merging region by simple addition, it turns out that at least the temperature dependence of the shape parameters changes drastically in this region compared to its behavior at lower temperatures. Depending on the assumptions made in the fitting procedure, changes also in the temperature dependence of the characteristic time scales and the strengths can be observed. In other words, it is not possible to consistently describe the total process as the addition of the two processes as extrapolated from the low temperature region. This could also be extracted as a conclusion from the recent work performed by Garwe *et al.* [11], where a nice study of the possible scenarios for the α-β splitting region is made. In our case, a just phenomenological scrutiny of the data discards the simple addition as a description of the experimental behavior: the strength of the β relaxation as measured below T_g, where it can be well determined without influence of the α relaxation, increases with temperature, whereas, from the above discussion, it should vanish above the merging. Therefore, another description of the merging process is clearly needed.

Taking into account the success of the evaluation of the NSE data as considering α and β relaxations as statistically independent processes, we are led to the same assumption for dielectric spectroscopy. Such an approach was in fact proposed by Williams a long time ago [13] but has never been quantitatively tested. As for the density fluctuations which are seen by the neutrons it is assumed that the polarization is partially relaxed via local motions, which conform the β relaxation. While the dipoles are participating in these motions, they are surrounded by temporary local environments. The collapse of these local environments is what we call α process, and causes the subsequently total relaxation of the polarization. Note that as the atoms in the density fluctuations all dipoles participate at the same time in both relaxation processes. Similar to the dynamic structure factor $S^{\alpha\beta}(Q,t)$ [Eq. (36)] the relaxation function $\varphi(t)$ corresponding to these two independent processes α,β, can be expressed as

$$\varphi(t)=f_\alpha\varphi_\alpha(t)+(1-f_\alpha)\varphi_\alpha(t)\varphi_\beta(t), \tag{38}$$

where f_α is the relative strength factor for the α process, and $\varphi_\alpha(t),\varphi_\beta(t)$ are the relaxation functions corresponding to the α and β processes. These are normalized functions, i.e., $\varphi_{\alpha(\beta)}(t=0)=1$, $\varphi_{\alpha(\beta)}(t=\infty)=0$. Note that Eq. (38) has the same form as $S^{\alpha\beta}(Q,t)$. However, while the neutron experiment occurs on the length scale of the α relaxation leading to a dispersive Q-dependent characteristic time, dielectric spectroscopy observes the effect of the different relaxation modes on a local probe—the dipole. Therefore also the prefactors in Eq. (38), which in the case of neutrons relate to particular Fourier transformed density-density correlations observed on their natural scale, have a different meaning, f_α being the relative fraction of the polarization relaxed only by the α relaxation.

For analyzing the experimental data, which are obtained in the frequency domain, we have to make use of the connection between dielectric permitivity and relaxation function in the time domain, which is via the Laplace transformation

$$\frac{\varepsilon^*(\omega)-\varepsilon_S}{\varepsilon_S-\varepsilon_\infty}=\Phi^*(\omega)=\mathbf{L}\left[-\frac{d\varphi(t)}{dt}\right]. \tag{39}$$

Here $\Phi^*(\omega)$ is the response function and ε_S and ε_∞ the zero and infinitive frequency limits of the real part of the dielectric function.

In order to apply the above described approach to the experimental data, first we have to determine the functional forms of $\varphi_\alpha(t)$ and $\varphi_\beta(t)$ [equivalently, of the response functions $\Phi^*_\alpha(\omega)$ and $\Phi^*_\beta(\omega)$]. Note that, if the time scales of the relaxation processes are well separated, $\varphi_\alpha(t)$ does not begin to decay until $\varphi_\beta(t)$ has completely vanished, $\varphi(t)$ decays in two stages and Eq. (38) can be approximated by

$$\varphi(t)\cong f_\alpha\varphi_\alpha(t)+(1-f_\alpha)\varphi_\beta(t), \tag{40}$$

i.e., under this condition we recover the usual description in terms of the addition of both contributions. Therefore, the functional forms of $\varphi_\alpha(t)$ and $\varphi_\beta(t)$ [$\Phi^*_\alpha(\omega)$ and $\Phi^*_\beta(\omega)$] can be obtained from the usual analysis of the low temperature region spectra, where the time scale of the α process is much slower than the one of the β process.

Once one knows how to describe both relaxations in its ''pure'' form, the difficulty of applying this formulation in

the merging region to the experimental data is that it involves a product in the time domain, which via Eq. (39) implies some kind of convolution in the frequency domain. In order to avoid Laplace transformations, either from the time derivative of the product of the theoretical functions into the frequency domain, or inversely from the experimental data in the time domain, we used the following procedure. It is useful to rewrite Eq. (38) as

$$\varphi(t)=f_\alpha\varphi_\alpha(t)+(1-f_\alpha)\varphi_{\beta\,\mathrm{eff}}(t). \tag{41}$$

Here, we are introducing the concept of the relaxation function of the ''effective β relaxation,'' $\varphi_{\beta\mathrm{eff}}(t)$, given by the product $\varphi_\alpha(t)\varphi_\beta(t)$. The formulation shown in Eq. (41) has the advantage that the total relaxation function is still given by the addition of two contributions, the one corresponding to the α relaxation, and the other by this ''effective β relaxation.'' This last includes the modifications of the β relaxation by the presence of the α relaxation. The total response function in the frequency domain will be given in terms of the response functions of the α and the effective β relaxation $\Phi^*_\alpha(\omega)$ and $\Phi^*_{\beta\,\mathrm{eff}}(\omega)$: so that we can write

$$\frac{\varepsilon^*(\omega)-\varepsilon_s}{\varepsilon_s-\varepsilon_\infty}=f_\alpha\Phi^*_\alpha(\omega)+(1-f_\alpha)\Phi^*_{\beta\,\mathrm{eff}}(\omega). \tag{42}$$

For calculating $\Phi^*_{\beta\,\mathrm{eff}}(\omega)$ we will make use of the fact that the relaxation functions $\varphi_\alpha(t)$ and $\varphi_\beta(t)$ can always be expressed in terms of superpositions of Debye processes with distributions of relaxation times $g_\alpha(\ln\tau)$ and $g_\beta(\ln\tau)$, respectively

$$\varphi_{\alpha(\beta)}(t)=\int_{-\infty}^{+\infty}g_{\alpha(\beta)}(\ln\tau)\exp\left(-\frac{t}{\tau}\right)d(\ln\tau). \tag{43}$$

The relaxation function $\varphi_{\beta\mathrm{eff}}(t)$ can be written as

$$\begin{aligned}\varphi_{\beta\,\mathrm{eff}}(t)=\varphi_\alpha(t)\varphi_\beta(t)&=\int_{-\infty}^{+\infty}g_\alpha(\ln\tau)\exp\left(-\frac{t}{\tau}\right)d(\ln\tau)\\&\times\int_{-\infty}^{+\infty}g_\beta(\ln\tau')\exp\left(-\frac{t}{\tau'}\right)d(\ln\tau')\\&=\int_{-\infty}^{+\infty}g_\alpha(\ln\tau)\left\{\int_{-\infty}^{+\infty}g_\beta(\ln\tau')\right.\\&\left.\times\exp\left[-t\left(\frac{1}{\tau'}+\frac{1}{\tau}\right)\right]d(\ln\tau')\right\}d(\ln\tau)\end{aligned} \tag{44}$$

and, taking into account the properties of the Laplace transformation, $\varphi^*_{\beta\,\mathrm{eff}}(\omega)$ is given by

$$\begin{aligned}\Phi^*_{\beta\,\mathrm{eff}}(\omega)=&\int_{-\infty}^{+\infty}g_\alpha(\ln\tau)\\&\times\left\{\int_{-\infty}^{+\infty}g_\beta(\ln\tau')\,\frac{1}{1+i\omega\left(\frac{1}{\tau'}+\frac{1}{\tau}\right)^{-1}}\,d(\ln\tau')\right\}\\&\times d(\ln\tau).\end{aligned} \tag{45}$$

In this way, $\Phi^*_{\beta\,\mathrm{eff}}(\omega)$ can be calculated by integration, avoiding any kind of Laplace transformation.

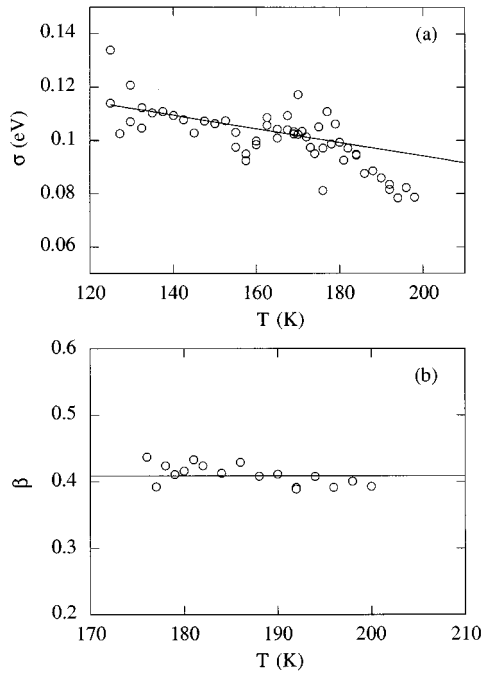

FIG. 12. Temperature dependence of the width of the distribution of barrier heights σ of the β relaxation (a) and the KWW shape parameter of the α relaxation (b) obtained from dielectric spectroscopy. Solid lines show the fit of σ in the low temperature range to a linear law in (a) and the mean value of β in (b).

VIII. DIELECTRIC STUDY: EVALUATION

As we have explained in the preceding section, the first step of the analysis consists of obtaining a description of the relaxation functions of the pure relaxations $\varphi_\alpha(t)$ and $\varphi_\beta(t)$ [equivalently, of the response functions $\Phi^*_\alpha(\omega)$ and $\Phi^*_\beta(\omega)$] from the temperature region where α and β relaxations are well separated in frequency and Eq. (40) can be considered a good approximation of Eq. (38). The results of this analysis are the following: as we have already mentioned, for describing the β relaxation we can use a superposition of Debye processes with a log-normal distribution of energy barrier heights, which in the frequency domain reads

$$\Phi^*_\beta(\omega)=\int_0^\infty g(E)\,\frac{1}{1+i\omega\tau_0\exp\left(\frac{E}{kT}\right)}\,dE, \tag{46}$$

where the distribution function $g(E)$ is given by Eq. (32b). The temperature dependence of the width of this distribution is shown in Fig. 12(a).

Concerning the α relaxation, a KWW functional form [17] was used for describing the relaxation function in the time domain,

$$\varphi_\alpha(t)=\exp\left[-\left(\frac{t}{\tau_{KWW}}\right)^\beta\right], \tag{47}$$

where β is the shape parameter and τ_{KWW} the characteristic time. This function does not have an analytical Laplace transform. However, it has been shown [29] that the Laplace transform of KWW functions can be well described by

Havriliak-Negami (HN) [30] functions if its shape parameters fulfill certain relationships. Therefore, for expressing the response function of the α relaxation in the frequency domain we made use of HN functions

$$\Phi^*_\alpha(\omega)=\frac{1}{[1+(i\omega\tau_{HN})^\alpha]^\gamma}, \tag{48}$$

where α and γ are the shape parameters and $\tau_{\rm HN}$ is the characteristic time, and we restricted ourselves to the HN-family functions which describe well the Laplace transform of KWW functions [29]. In these cases, the relationships between HN- and KWW-shape parameters and their characteristic times are [31]

$$\alpha\gamma=\beta^{1.23}, \tag{49a}$$

$$\log\left[\frac{\tau_{HN}}{\tau_{KWW}}\right]=2.6(1-\beta)^{0.5}\exp(-3\beta). \tag{49b}$$

The values of the shape parameter β obtained for PB are shown in Fig. 12(b). They lie around a mean value of β=0.41. The corresponding HN shape parameters are α=0.72, γ=0.50. As can be realized in this figure, the spectra were analyzed in this way in the temperature range between T_g and T_g+22 K, where we could consider that the time scales of α and β relaxations are separated enough (see Fig. 11). However, we can see that in the case of the shape parameter of the β relaxation already at $\approx T_g$+5 K deviations from the behavior deduced from lower temperatures can be observed. These deviations will be understandable later. Although the temperature dependence of the other free parameter of the fit $\tau_{\rm HN}$ (equivalently, $\tau_{\rm KWW}$) could be described by a Vogel-Fulcher (VF) law, the accuracy in the determination of the VF parameters is very low. This is a consequence of the narrow temperature range in which the characteristic timescale of the α relaxation is determined by this analysis.

At temperatures close and above the merging we applied the formalism described in Sec. VII: the experimental data were fitted to Eq. (42) with help of Eq. (45). The distribution $g_\alpha(\ln\tau)$ was obtained by using an algorithm proposed by Imanishi, Adachi, and Kotaka [32]; the procedure followed is the same as explained in [29,31]. The function $g_\beta(\ln\tau)$ can easily be obtained from the distribution of energy barrier heights $g(E)$ [Eq. (32b)]

$$g_\beta(\ln\,\tau)=\frac{kT}{\sqrt{\pi}\,\sigma}\exp\left[-\left(\frac{kT\,\ln\left(\frac{\tau}{\tau_0}\right)-E_0}{\sigma}\right)^2\right]. \tag{50}$$

Note that, except for $\tau_{\rm HN}$ (equivalently, $\tau_{\rm KWW}$) and the relaxed fraction in the α relaxation f_α, which were left as free parameters in the fitting procedure, all the parameters were extrapolated from the low to the high temperature regime. We found a very good description of the data by this procedure, as can be seen in Fig. 10, for the whole range of temperatures investigated. Moreover, a very interesting result concerning the time scale of the α relaxation, $\tau_{\rm HN}$, arises from this analysis: its temperature behavior at high temperatures follows very nicely the temperature behavior of the time scale associated with the viscosity (see Fig. 13). This is a nontrivial result which emerges naturally from the description made and supports the consistency of the analysis of the data, if we take into account that the same temperature dependence has been found for the characteristic time scale of the α relaxation as observed by NSE.

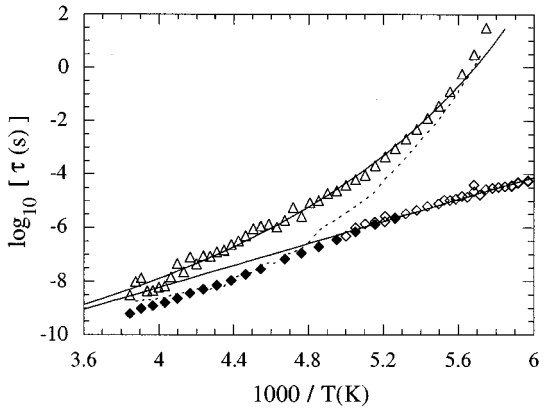

FIG. 13. Temperature dependence of the dielectric characteristic times obtained by the fitting procedure explained in the text: $\tau_{\rm HN}$ (△), $\tau^{\beta}_{\rm max}$ (◇), and $\tau^{\beta\,\rm eff}_{\rm max}$ (◆). The Arrhenius law shows the extrapolation of the temperature behavior of the β relaxation. The solid line through $\tau_{\rm HN}$ points shows the temperature behavior of the time scale associated to the viscosity. The dotted line corresponds to the temperature dependence of the characteristic time scales for the main relaxation process.

Figure 14 shows the behavior obtained for the relative fraction relaxed only by the α relaxation f_α. This magnitude decreases with increasing temperature, being small at temperatures close to the merging. Unfortunately, the quality of the high frequency data does not allow us to precisely determine the values of this parameter at high temperatures, but it can be supposed to be very small or 0 above the merging. As above mentioned, this lack of accuracy is due to the low value of the dipole moment of our sample.

We would like to remark that the result obtained that f_α vanishes or takes low values at high temperatures does not mean that the dipoles do not participate anymore in the α relaxation. In our approach all the dipoles are involved simultaneously in both, α and β processes. What this result implies is that at high temperatures all or almost all the po-

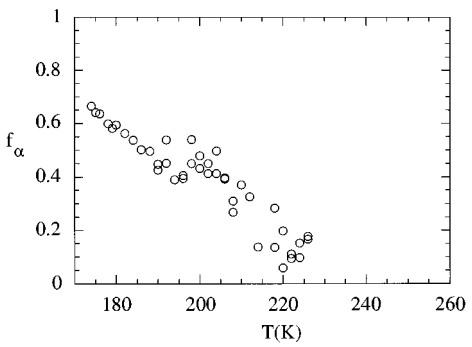

FIG. 14. Fraction of the polarization relaxed through the α relaxation as a function of temperature.

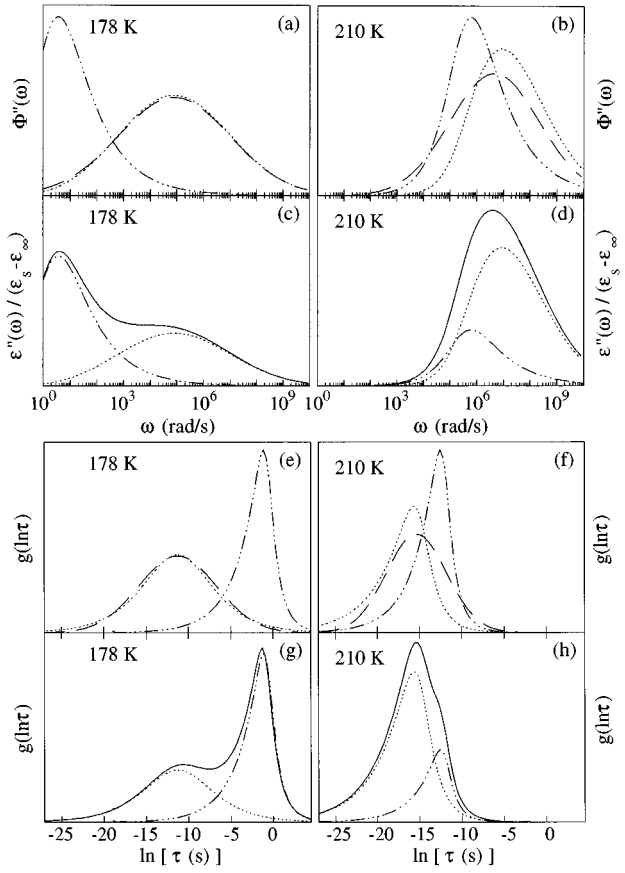

FIG. 15. Imaginary part of the response function (a), (b), dielectric loss (c), (d), and distribution of relaxation times (e), (f), (g), (h) corresponding to the α relaxation (dashed-dotted lines), the β relaxation (dashed lines), the effective β relaxation (dotted lines), and the total relaxation (solid lines) at the two temperatures indicated. In (c), (d), (g), and (h) the dashed-dotted and the dotted lines represent the contributions of the α relaxation and the effective β relaxation, respectively, to the total corresponding function.

larization decays through what we have called effective β relaxation, which accounts for both, primary and secondary relaxations. In order to clarify the meaning of this ''fictive'' relaxation, Fig. 15 shows how the α, and β, and the effective β relaxations behave with temperature. As can be seen in Fig. 15(a), at T_g, where the time scales of α and β process are separated by four or five orders of magnitude, $\Phi''_{\beta}(\omega)$ and $\Phi''_{\beta\text{eff}}(\omega)$ are almost indistinguishable. Also the corresponding distribution functions of relaxation times are almost identical [Fig. 15(e)]. However, as the temperature increases and the time scales of α and β relaxations become closer, we can find significant changes not only in the shape but also in the frequency of the maximum of $\Phi''_{\beta\text{eff}}(\omega)$ with respect to $\Phi''_{\beta}(\omega)$ [see an example in Fig. 15(b), just in the merging region]. The effect of the proximity of the α process on $\Phi''_{\beta\text{eff}}(\omega)$ consists of an asymmetrization of this function and a shift of its characteristic time scale towards higher frequencies. The reason of this resulting effect is evidenced in Fig. 15(f), where the distribution functions of relaxation times are shown. We can see that the β-like processes with characteristic times slower than the average relaxation time of the α relaxation do not contribute anymore to the relaxation of the polarization; this means that the dipoles whose local environment relaxes before the local dynamics takes place, relax through the α relaxation. The higher the temperature, the more similar becomes the shape of the distribution function of relaxation times of the effective β relaxation to the shape of the distribution function of relaxation times of the α relaxation, but shifted in the ln τ axis.

The imaginary part of the response function and the distribution of relaxation times of the total process at 178 K and 210 K are shown in Figs. 15(c), 15(d), 15(g), and 15(h), respectively. Here we can see the relative contributions of the α and effective β relaxations to these functions: close to T_g, the α relaxation alone plays the most important role, whereas in the merging region almost all the relaxation of the polarization is due to the other mechanism (local processes together with the α relaxation). It is noteworthy to remark that the description found for the elemental process beyond the secondary relaxation from the NSE evaluation is compatible with the dielectric results. Rotations of the *cis* unit of about 60°–120° would allow the polarization to relax to a large extent, leaving a small fraction to be relaxed only via the pure α segmental process.

The behavior obtained for the effective β relaxation explains why the σ parameter (shape parameter of the β relaxation) resulting from the analysis of the data as simple addition deviates close to T_g from the extrapolated behavior towards smaller values: the effect of the asymmetrization of the response function of the β relaxation becomes nonnegligible in this temperature range. On the other hand, we can understand in the light of this description why the temperature behavior of the total process does not follow at high temperatures the behavior of the characteristic time scale associated to the viscosity, which is in fact the behavior found for the pure α relaxation. As we have mentioned, the maxima of $\Phi''_{\beta\text{eff}}(\omega)$ do not coincide with the maxima of $\Phi''_{\beta}(\omega)$, but they occur at higher frequency. In Fig. 13 we have plotted for several temperatures the inverse of the frequencies of the maxima of $\Phi''_{\beta}(\omega)$. We know now that the dominating role in the relaxation of the polarization at high temperatures is played by the local dynamics together with the α relaxation and not by only the α relaxation alone, and therefore the temperature dependence of the total process follows the temperature dependence of the effective β relaxation, as is shown in Fig. 13. In this way, we have a simple explanation of this up to now not clarified behavior.

IX. CONCLUSIONS

We have investigated the local dynamics of 1,4 PB in the temperature region below and above the merging of the structural α and secondary β relaxations using NSE and dielectric spectroscopy. Thereby, we have consequently exploited the complementary strengths of both methods. While dielectric spectroscopy yields very precise information on the temporal evolution of the relaxations, NSE provides space and time resolution on the length and time scales in question. The combined results of both techniques yielded a deeper understanding of the motional processes behind the relaxations.

Exploiting the Q dependence of the coherent dynamic structure factor as measured by NSE it became possible (i) at

temperatures below the merging temperature T_M to obtain spatial information on the chain motions behind the β relaxation. The results suggest rotational motion of the chain building blocks like *cis* and *trans* units within one chain, stressing the intramolecular nature of this process. In order to facilitate the analysis it was of crucial importance to use the distribution function of the elemental relaxation processes provided by the dielectric results. (ii) At temperatures around T_M and above the NSE experiments qualified the α relaxation as being mainly related to interchain motions. Its detailed time dependence, thereby, does perfectly agree with the dielectric line shapes of the α process. (iii) The dynamic structure factor above T_M can consistently be described assuming that α and β relaxations in 1,4 PB are statistically independent processes.

Taking into account this last conclusion as an input for the analysis of the dielectric results it has been possible: (iv) to describe the dielectric response in the α-β merging and above starting from the low temperature behavior of the α and β processes and without considering any particular change on the relaxation mechanism of these processes. (v) To clarify the discrepancy between the temperature dependence of the viscosity and the inverse of the frequency of the dielectric maxima, which is observed at high temperatures above the merging region. (vi) Last but not least we would like to point out that we have developed a mathematical procedure for analyzing the frequency domain dielectric data in the framework of the above mentioned ideas. These conclusions, so far, are specific for 1,4 PB, and it will be of great interest to investigate whether or not they can be generalized for other glass-forming polymer systems.

ACKNOWLEDGMENTS

We acknowledge partial support by the HCM-EC project (Contract: ERBCHRXCT 920009), and the Acciones Integradas Spain-Germany (Contract: AI 95-09). Financial support from the Spanish CICyT, project MEC PB94-0468 is acknowledged by J.C.; A.A. also acknowledges the EC-Grant (Contract: ERBCHBGCT940603). We are thankful to Professor U. Buchenau, Professor E. W. Fischer, and Professor A. Patkowski for helpful discussions, and to Professor A. Alegría and Dr. M. Monkenbusch for experimental help.

[1] See, e.g., N. G. McCrum, B. E. Read, and G. Williams, in *Anelastic and Dielectric Effects in Polymer Solids* (Wiley, London, 1967).
[2] See, e.g., *Dynamics on Disordered Materials II*, edited by A. J. Dianoux, W. Petry, and D. Richter (North-Holland, Amsterdam, 1993).
[3] G. P. Johari and M. Goldstein, J. Chem. Phys. **53**, 2372 (1970).
[4] W. Götze, in *Liquids, Freezing and the Glass Transition*, edited by J. P. Hansen, D. Levesque, J. Zinn-Justin (North-Holland, Amsterdam, 1991).
[5] F. Mezei, W. Knaak, and B. Farago, Phys. Rev. Lett. **58**, 571 (1987).
[6] D. Richter, B. Frick, and B. Farago, Phys. Rev. Lett. **61**, 2465 (1988).
[7] D. Richter, R. Zorn, B. Farago, B. Frick, and L. J. Fetters, Phys. Rev. Lett. **68**, 71 (1992).
[8] R. Zorn (unpublished).
[9] A. Arbe, U. Buchenau, L. Willner, D. Richter, B. Farago, and J. Colmenero, Phys. Rev. Lett. **76**, 1872 (1996).
[10] B. Frick, D. Richter, and Cl. Ritter, Europhys. Lett. **9**, 557 (1989).
[11] F. Garwe, A. Schönhals, H. Lockwenz, M. Beiner, K. Schröter, and E. Donth, Macromolecules **29**, 247 (1996).
[12] A. Hofmann, A. Alegría, J. Colmenero, L. Willner, E. Buscaglia, and N. Hadjichristidis, Macromolecules **29**, 129 (1996).
[13] See, e.g., G. Williams, Adv. Polymer Sci. **33**, 60 (1979).
[14] See, e.g., *Neutron Spin Echo*, edited by F. Mezei, Lecture Notes in Physics Vol. 28 (Springer-Verlag, Heidelberg, 1980).
[15] G. Vineyard, Phys. Rev. **110**, 999 (1959).
[16] M. Morton and L. J. Fetters, Rubber Rev. **48**, 359 (1975).
[17] F. Kohlrausch, Pogg. Ann. Phys. **119**, 352 (1863); G. Williams and D. C. Watts, Trans. Faraday Soc. **66**, 80 (1970).
[18] $\xi(T)=\xi_0\exp[1/\alpha(T-T_0)]$, with $\xi_0=1.26\times10^{-11}$ dyn sec/cm, $T_0=128$ K, and $\alpha=7.12\times10^{-4}$ K [G. C. Berry and T. G. Fox, Adv. Polym. Sci. **5**, 261 (1968)].
[19] K. S. Cole and R. H. Cole, J. Chem. Phys. **9**, 341 (1941).
[20] See, e.g., L. Wu and S. R. Nagel, Phys. Rev. B **46**, 11 198 (1992).
[21] V. G. Karpov, M. I. Klinger, and F. N. Ignat'ev, Zh. Eksp. Teor. Fiz. **84**, 760 (1983) [Sov. Phys JETP **57**, 439 (1983)].
[22] C. Dreyfus, A. Aoudi, R. Pick, A. Patkowski, W. Steffen, B. Strube, and E. W. Fischer (unpublished).
[23] R. D. Deegan and S. R. Nagel, Phys. Rev. B **52**, 5653 (1995).
[24] See, e.g., P. J. Flory, in *Statistical Mechanics of Chain Molecules* (Wiley, New York, 1969).
[25] R. Zorn, A. Arbe, J. Colmenero, B. Frick, D. Richter, and U. Buchenau, Phys. Rev. E **52**, 781 (1995).
[26] P. G. de Gennes, Physica **25**, 825 (1959).
[27] R. Zorn, D. Richter, B. Frick, and B. Farago, Physica A **201**, 52 (1993).
[28] A. L. McLellan, in *Tables of Experimental Dipole Moments* (Freeman, San Francisco, 1963).
[29] F. Alvarez, A. Alegría, and J. Colmenero, Phys. Rev. B **47**, 125 (1993).
[30] S. Havriliak and S. Negami, Polymer **8**, 161 (1967).
[31] F. Alvarez, A. Alegría, and J. Colmenero, Phys. Rev. B **44**, 7306 (1991).
[32] Y. Imanishi, K. Adachi, and T. Kotaka, J. Chem. Phys. **89**, 7593 (1988).